

A statistical framework for powerful multi-trait rare variant analysis in large-scale whole-genome sequencing studies

Xihao Li^{1,2}, Han Chen^{3,4}, Margaret Sunitha Selvaraj^{5,6,7}, Eric Van Buren⁸, Hufeng Zhou⁸, Yuxuan Wang⁹, Ryan Sun¹⁰, Zachary R. McCaw¹, Zhi Yu^{5,6,7}, Donna K. Arnett¹¹, Joshua C. Bis¹², John Blangero¹³, Eric Boerwinkle^{3,14}, Donald W. Bowden¹⁵, Jennifer A. Brody¹², Brian E. Cade^{6,16,17}, April P. Carson¹⁸, Jenna C. Carlson¹⁹, Nathalie Chami²⁰, Yii-Der Ida Chen²¹, Joanne E. Curran¹³, Paul S. de Vries³, Myriam Fornage^{3,22}, Nora Franceschini²³, Barry I. Freedman²⁴, Charles Gu²⁵, Nancy L. Heard-Costa^{26,27}, Jiang He^{28,29}, Lifang Hou³⁰, Yi-Jen Hung³¹, Marguerite R. Irvin³², Robert C. Kaplan^{33,34}, Sharon L.R. Kardia³⁵, Tanika Kelly³⁶, Iain Konigsberg³⁷, Charles Kooperberg³⁴, Brian G. Kral³⁸, Changwei Li^{28,29}, Ruth J.F. Loos^{20,39}, Michael C. Mahaney¹³, Lisa W. Martin⁴⁰, Rasika A. Mathias³⁸, Ryan L. Minster¹⁹, Braxton D. Mitchell⁴¹, May E. Montasser⁴¹, Alanna C. Morrison³, Nicholette D. Palmer¹⁵, Patricia A. Peyser³⁵, Bruce M. Psaty^{12,42,43}, Laura M. Raffield², Susan Redline^{16,17}, Alexander P. Reiner^{34,42}, Stephen S. Rich⁴⁴, Colleen M. Sitlani¹², Jennifer A. Smith³⁵, Kent D. Taylor²¹, Hemant Tiwari⁴⁵, Ramachandran S. Vasan^{27,46}, Zhe Wang²⁰, Lisa R. Yanek³⁸, Bing Yu³, NHLBI Trans-Omics for Precision Medicine (TOPMed) Consortium, Kenneth M. Rice⁴⁷, Jerome I. Rotter²¹, Gina M. Peloso⁹, Pradeep Natarajan^{5,6,7}, Zilin Li^{8,*}, Zhonghua Liu^{48,*} and Xihong Lin^{6,8,49*}

¹Department of Biostatistics, University of North Carolina at Chapel Hill, Chapel Hill, NC, USA.

²Department of Genetics, University of North Carolina at Chapel Hill, Chapel Hill, NC, USA.

³Human Genetics Center, Department of Epidemiology, Human Genetics, and Environmental Sciences, School of Public Health, The University of Texas Health Science Center at Houston, Houston, TX, USA.

⁴Center for Precision Health, School of Biomedical Informatics, The University of Texas Health Science Center at Houston, Houston, TX, USA.

⁵Center for Genomic Medicine and Cardiovascular Research Center, Massachusetts General Hospital, Boston, MA, USA.

⁶Program in Medical and Population Genetics, Broad Institute of Harvard and MIT, Cambridge, MA, USA.

⁷Department of Medicine, Harvard Medical School, Boston, MA, USA.

⁸Department of Biostatistics, Harvard T.H. Chan School of Public Health, Boston, MA, USA.

⁹Department of Biostatistics, Boston University School of Public Health, Boston, MA, USA.

¹⁰Department of Biostatistics, University of Texas MD Anderson Cancer Center, Houston, TX, USA.

¹¹Provost Office, University of South Carolina, Columbia, SC, USA.

¹²Cardiovascular Health Research Unit, Department of Medicine, University of Washington, Seattle, WA, USA.

¹³Department of Human Genetics and South Texas Diabetes and Obesity Institute, School of Medicine, The University of Texas Rio Grande Valley, Brownsville, TX, USA.

¹⁴Human Genome Sequencing Center, Baylor College of Medicine, Houston, TX, USA.

¹⁵Department of Biochemistry, Wake Forest University School of Medicine, Winston-Salem, NC, USA.

¹⁶Division of Sleep and Circadian Disorders, Brigham and Women's Hospital, Boston, MA, USA.

¹⁷Division of Sleep Medicine, Harvard Medical School, Boston, MA, USA.

¹⁸Department of Medicine, University of Mississippi Medical Center, Jackson, MS, USA.

¹⁹Department of Human Genetics and Department of Biostatistics, University of Pittsburgh, Pittsburgh, PA, USA.

²⁰The Charles Bronfman Institute for Personalized Medicine, Icahn School of Medicine at Mount Sinai, New York, NY, USA.

²¹The Institute for Translational Genomics and Population Sciences, Department of Pediatrics, The Lundquist Institute for Biomedical Innovation at Harbor-UCLA Medical Center, Torrance, CA, USA.

²²Brown Foundation Institute of Molecular Medicine, McGovern Medical School, the University of Texas Health Science Center at Houston, Houston, TX, USA.

²³Department of Epidemiology, University of North Carolina at Chapel Hill, Chapel Hill, NC, USA.

²⁴Department of Internal Medicine, Nephrology, Wake Forest University School of Medicine, Winston-Salem, NC, USA.

²⁵Division of Biology & Biomedical Sciences, Washington University School of Medicine, St. Louis, MO, USA.

²⁶Department of Neurology, Boston University Chobanian & Avedisian School of Medicine, Boston, MA, USA.

²⁷Framingham Heart Study, Framingham, MA, USA.

²⁸Department of Epidemiology, Tulane University School of Public Health and Tropical Medicine, New Orleans, LA, USA.

²⁹Tulane University Translational Science Institute, New Orleans, LA, USA.

³⁰Department of Preventive Medicine, Northwestern University, Chicago, IL, USA.

³¹Department of Internal Medicine, Tri-Service General Hospital, National Defense Medical Center, Taipei, Taiwan.

³²Department of Epidemiology, School of Public Health, University of Alabama at Birmingham, Birmingham, AL, USA.

³³Department of Epidemiology and Population Health, Albert Einstein College of Medicine, Bronx, NY, USA.

³⁴Division of Public Health Sciences, Fred Hutchinson Cancer Center, Seattle, WA, USA.

³⁵Department of Epidemiology, School of Public Health, University of Michigan, Ann Arbor, MI, USA.

³⁶Department of Medicine, Division of Nephrology, University of Illinois Chicago, Chicago, IL, USA.

³⁷Department of Biomedical Informatics, University of Colorado, Aurora, CO, USA.

³⁸Department of Medicine, Johns Hopkins University School of Medicine, Baltimore, MD, USA.

³⁹Novo Nordisk Foundation Center for Basic Metabolic Research, Faculty of Health and Medical Sciences, University of Copenhagen, Copenhagen, Denmark.

⁴⁰George Washington University School of Medicine and Health Sciences, Washington, DC, USA.

⁴¹Department of Medicine, University of Maryland School of Medicine, Baltimore, MD, USA.

⁴²Departments of Epidemiology, University of Washington, Seattle, WA, USA.

⁴³Department of Health Systems and Population Health, University of Washington, Seattle, WA, USA.

⁴⁴Center for Public Health Genomics, University of Virginia, Charlottesville, VA, USA.

⁴⁵Department of Biostatistics, School of Public Health, University of Alabama at Birmingham, Birmingham, AL, USA.

⁴⁶Department of Quantitative and Qualitative Health Sciences, UT Health San Antonio School of Public Health, San Antonio, TX, USA.

⁴⁷Department of Biostatistics, University of Washington, Seattle, WA, USA.

⁴⁸Department of Biostatistics, Mailman School of Public Health, Columbia University, New York, NY, USA.

⁴⁹Department of Statistics, Harvard University, Cambridge, MA, USA.

*Correspondence should be addressed to Z. Li (li@hsp.harvard.edu), Z. Liu (zl2509@cumc.columbia.edu) and X. Lin (xlin@hsp.harvard.edu).

List of consortium members and their affiliations appears at the end of the paper.

1 **Abstract**

2 Large-scale whole-genome sequencing (WGS) studies have improved our
3 understanding of the contributions of coding and noncoding rare variants to complex
4 human traits. Leveraging association effect sizes across multiple traits in WGS rare
5 variant association analysis can improve statistical power over single-trait analysis, and
6 also detect pleiotropic genes and regions. Existing multi-trait methods have limited
7 ability to perform rare variant analysis of large-scale WGS data. We propose
8 MultiSTAAR, a statistical framework and computationally-scalable analytical pipeline for
9 functionally-informed multi-trait rare variant analysis in large-scale WGS studies.
10 MultiSTAAR accounts for relatedness, population structure and correlation among
11 phenotypes by jointly analyzing multiple traits, and further empowers rare variant
12 association analysis by incorporating multiple functional annotations. We applied
13 MultiSTAAR to jointly analyze three lipid traits (low-density lipoprotein cholesterol, high-
14 density lipoprotein cholesterol and triglycerides) in 61,861 multi-ethnic samples from the
15 Trans-Omics for Precision Medicine (TOPMed) Program. We discovered new
16 associations with lipid traits missed by single-trait analysis, including rare variants within
17 an enhancer of *NIPSNAP3A* and an intergenic region on chromosome 1.

18

19

20

21

22

23

24 Advances in next generation sequencing technologies and the decreasing cost of
25 whole-exome/whole-genome sequencing (WES/WGS) have made it possible to study
26 the genetic underpinnings of rare variants (i.e. minor allele frequency (MAF) < 1%) in
27 complex human traits. Large nationwide consortia and biobanks, such as the National
28 Heart, Lung and Blood Institute (NHLBI)'s Trans-Omics for Precision Medicine
29 (TOPMed) Program¹, the National Human Genome Research Institute's Genome
30 Sequencing Program (GSP) , the National Institute of Health's All of Us Research
31 Program², and the UK's Biobank WGS Program³, are expected to sequence more than
32 a million of individuals in total, at more than 1 billion genetic variants in both coding and
33 noncoding regions of the human genome, while also recording thousands of
34 phenotypes. To mitigate the lack of power of single-variant analyses to identify rare
35 variant associations⁴, variant set tests have been proposed to analyze the joint effects
36 of multiple rare variants ⁵⁻⁹, where most of the work has focused single trait analysis.

37
38 Pleiotropy occurs when genetic variants influence multiple traits¹⁰. There is growing
39 empirical evidence from genome-wide association studies (GWASs) that many variants
40 have pleiotropic effects^{11,12}. Identifying these effects can provide valuable insights into
41 the genetic architecture of complex traits¹³. As such, it is of increasing interest to identify
42 pleiotropic rare variants by jointly analyzing multiple traits in WGS rare variant
43 association studies (RVASs).

44
45 Several existing methods for multi-trait rare variant association analysis, such as
46 MSKAT¹⁴, Multi-SKAT¹⁵ and MTAR¹⁶, have shown that leveraging the cross-phenotype

47 correlation structure can improve the power of multi-trait analyses compared to single-
48 trait analyses when analyzing pleiotropic genes¹⁴⁻¹⁷. However, existing methods do not
49 scale well, and are not feasible when analyzing large-scale WGS studies with hundreds
50 of millions of rare variants in samples exhibiting relatedness and population structure.
51 Furthermore, none of the existing multi-trait rare variant analysis methods leverages
52 functional annotations that predict the biological functionality of variants, resulting in
53 limited interpretability and power loss. While the STAAR method¹⁸ dynamically
54 incorporates multiple variant functional annotations to maximize the power of rare
55 variant association tests, it is designed for single-trait analysis and cannot be directly
56 applied to multiple traits.

57
58 To overcome these limitations, we propose the Multi-trait variant-Set Test for
59 Association using Annotation infoRmation (MultiSTAAR), a statistical framework for
60 multi-trait rare variant analyses of large-scale WGS studies and biobanks. It has several
61 features. First, by fitting a null Multivariate Linear Mixed Model (MLMM)¹⁹ for multiple
62 quantitative traits simultaneously, adjusting for ancestry principal components (PCs)²⁰
63 and using a sparse genetic relatedness matrix (GRM)^{21,22}, MultiSTAAR scales well but
64 also accounts for relatedness and population structure, as well as correlations among
65 the multiple traits. Second, MultiSTAAR enables the incorporation of multiple variant
66 functional annotations as weights to improve the power of RVASs. Furthermore, we
67 provide MultiSTAAR via a comprehensive pipeline for large-scale WGS studies, that
68 facilitates functionally-informed multi-trait analysis of both coding and noncoding rare

69 variants. Third, MultiSTAAR enables conditional multi-trait analysis to assess rare
70 variant association signals beyond known common and low frequency variants.

71
72 In the current study, we conducted extensive simulation studies to demonstrate the
73 validity of MultiSTAAR and to assess the power gain of MultiSTAAR by incorporating
74 multiple relevant variant functional annotations, and its ability in preserving Type I error
75 rates. We then applied MultiSTAAR to perform WGS RVAS of 61,838 ancestrally
76 diverse participants from 20 studies from NHLBI's TOPMed consortium by jointly
77 analyzing three circulating lipid traits: low-density lipoprotein cholesterol (LDL-C), high-
78 density lipoprotein cholesterol (HDL-C) and triglycerides (TG). We show that
79 MultiSTAAR is computationally feasible for large-scale WGS multi-trait rare variant
80 analysis, and in conditional analysis of LDL-C, HDL-C and TG, MultiSTAAR identifies
81 signals that were missed either by the existing multi-trait rare variant analysis methods
82 that overlook variant functional annotations, or by single-trait functionally-informed
83 analysis that ignore correlations between phenotypes.

84

85 **Results**

86 **Overview of the methods**

87 MultiSTAAR is a statistical framework and an analytic pipeline for jointly analyzing
88 multiple traits in large-scale WGS rare variant association studies. There are two main
89 components in the MultiSTAAR framework: (i) fitting null MLMMs using ancestry PCs
90 and sparse GRMs to account for population structure, relatedness and the correlation
91 between phenotypes, and (ii) testing for associations between each aggregated variant

92 set and multiple traits by dynamically incorporating multiple variant functional
93 annotations¹⁸ (**Fig. 1a**).
94
95 In WGS RVASs, an important but often underemphasized challenge is selecting
96 biologically-meaningful and functionally-interpretable analysis units, especially for the
97 noncoding genome^{23,24}. In gene-centric analyses of multiple traits, MultiSTAAR provides
98 five functional categories (masks) to aggregate coding rare variants of each protein-
99 coding gene, as well as an additional eight masks of regulatory regions to aggregate
100 noncoding rare variants. In non-gene-centric analyses of multiple traits, MultiSTAAR
101 performs agnostic genetic region analyses using sliding windows^{18,25} (**Fig. 1b**).
102
103 For each rare variant set analyzed, MultiSTAAR first constructs the multi-trait burden,
104 SKAT and ACAT-V test statistics (**Methods**). For each type of rare variant test,
105 MultiSTAAR calculates multiple candidate *P* values using different variant functional
106 annotations as weights, following the STAAR framework¹⁸. MultiSTAAR then
107 aggregates the association strength by combining the *P* values from all annotations
108 using the ACAT method, that provides robustness to correlation between tests⁹, and
109 proposes an omnibus test, MultiSTAAR-O, that leverages the advantages of different
110 type of tests (**Methods**). Furthermore, MultiSTAAR can test multi-trait rare variants'
111 associations conditional on a set of known associations (**Fig. 1b**).
112
113 **Simulation studies**

114 To evaluate the type I error rates and the power of MultiSTAAR, we performed
115 simulation studies under several configurations. Following the steps described in Data
116 **Simulation (Methods)**, we generated three quantitative traits with a correlation matrix
117 similar to the empirical correlation in the three lipid traits²⁶⁻²⁸. We then generated
118 genotypes by simulating 20,000 sequences for 100 different 1 megabase (Mb) regions,
119 each of them were generated to mimic the linkage disequilibrium structure of an African
120 American population by using the calibration coalescent model²⁹. Throughout the
121 simulation studies, we randomly and uniformly selected 5-kilobase (kb) regions from
122 these 1-Mb regions and considered sample sizes of 10,000 for each replicate. The
123 simulation studies focused on aggregating uncommon variants with an MAF < 5%.

124

125 **Type I error rate evaluations**

126 We performed 10^8 simulations to evaluate the type I error rates of the multi-trait burden,
127 SKAT, ACAT-V and MultiSTAAR-O tests at $\alpha = 10^{-4}, 10^{-5}$, and 10^{-6} (**Supplementary**
128 **Table 1**). The results show that, for multi-trait rare variant analysis, all four MultiSTAAR
129 tests controlled the type I error rates at very close to the nominal α levels.

130

131 **Empirical power simulations**

132 We next assessed the power of MultiSTAAR-O for the analysis of multiple phenotypes
133 under different genetic architectures, while also comparing its power with existing
134 methods. Specifically, we considered four models, in which variants in the signal region
135 (variant-phenotype association regions) were associated with (1) one phenotype only,
136 (2) two positively correlated phenotypes, (3) two negatively correlated phenotypes and

137 (4) all three phenotypes. In addition, we considered different proportions (5%, 15% and
138 35% on average) of causal variants in the signal region, where causality of variants
139 depended on different sets of annotations, and the effect size directions of causal
140 variants were allowed to vary (**Methods**). Power was evaluated as the proportions of P
141 values less than $\alpha = 10^{-7}$ based on 10^4 simulations. Overall, MultiSTAAR-O
142 consistently delivered higher power to detect signal regions compared to multi-trait
143 burden, SKAT and ACAT-V tests, through its incorporation of multiple annotations
144 (**Extended Data Figs. 2-5, Supplementary Figs. 1-4**). This power advantage was also
145 robust to the existence of noninformative annotations.

146

147 **Application to the TOPMed lipids WGS data**

148 We applied MultiSTAAR to identify rare variant associations with three quantitative lipid
149 traits (LDL-C, HDL-C and TG) through a multi-trait analysis using TOPMed Freeze 8
150 WGS data, comprising 61,838 individuals from 20 multi-ethnic studies (**Supplementary**
151 **Note**). LDL-C values were adjusted for the usage of lipid-lowering medication^{26,30}
152 (**Methods**), and DNA samples were sequenced at >30x target coverage. Sample- and
153 variant-level quality control were performed for each participating study^{1,26,30}.

154

155 Race/ethnicity was measured using a combination of self-reported race/ethnicity and
156 study recruitment information³¹ (**Supplementary Note**). Of the 61,838 samples, 15,636
157 (25.3%) were Black or African American, 27,439 (44.4%) were White, 4,461 (7.2%)
158 were Asian or Asian American, 13,138 (21.2%) were Hispanic/Latino American and
159 1,164 (1.9%) were Samoans. There were 414 million single-nucleotide variants (SNVs)

160 observed overall, with 6.5 million (1.6%) common variants (MAF > 5%), 5.2 million
161 (1.2%) low-frequency variants (1% ≤ MAF ≤ 5%) and 402 million (97.2%) rare variants
162 (MAF < 1%). The study-specific demographics and baseline characteristics are given in
163 **Supplementary Table 2.**

164

165 **Gene-centric multi-trait analysis of coding and noncoding rare variants**

166 We applied MultiSTAAR-O on gene-centric multi-trait analysis of coding and noncoding
167 rare variants of genes with lipid traits in TOPMed. For coding variants, rare variants
168 (MAF < 1%) from five coding functional categories (masks) were aggregated,
169 separately, and analyzed using a joint model for LDL-C, HDL-C and TG, including (1)
170 putative loss-of-function (stop gain, stop loss and splice) rare variants, (2) missense
171 rare variants, (3) disruptive missense rare variants, (4) putative loss-of-function and
172 disruptive missense rare variants and (5) synonymous rare variants of each protein-
173 coding gene. The putative loss-of-function, missense and synonymous RVs were
174 defined by GENCODE Variant Effect Predictor (VEP) categories³². The disruptive
175 variants were further defined by MetaSVM³³, which measures the deleteriousness of
176 missense mutations. We incorporated 9 annotation principal components (aPCs)^{18,26,34},
177 CADD³⁵, LINSIGHT³⁶, FATHMM-XF³⁷ and MetaSVM³³ (for missense rare variants only)
178 along with the two MAF-based weights⁴ in MultiSTAAR-O (**Supplementary Table 3**).
179 The overall distribution of MultiSTAAR-O *P* values was well-calibrated for the multi-trait
180 analysis of coding rare variants (**Extended Data Fig. 1b**). At a Bonferroni-corrected
181 significance threshold of $\alpha = 0.05/(20,000 \times 5) = 5.00 \times 10^{-7}$, accounting for five
182 different coding masks across protein-coding genes, MultiSTAAR-O identified 51

183 genome-wide significant associations using unconditional multi-trait analysis (**Extended**
184 **Data Fig. 1a, Supplementary Table 4**). After conditioning on previously reported
185 variants associated with LDL-C, HDL-C or TG located within a 1 Mb broader region of
186 each coding mask in the GWAS Catalog and Million Veteran Program (MVP)^{26,38,39}, 34
187 out of the 51 associations remained significant at the Bonferroni-corrected threshold of
188 $\alpha = 0.05/51 = 9.80 \times 10^{-4}$ (**Table 1**).

189

190 For non-coding variants, rare variants from eight noncoding masks were analyzed in a
191 similar fashion, including (1) promoter rare variants overlaid with CAGE sites⁴⁰, (2)
192 promoter rare variants overlaid with DHS sites⁴¹, (3) enhancer rare variants overlaid
193 with CAGE sites^{42,43}, (4) enhancer rare variants overlaid with DHS sites^{41,43}, (5)
194 untranslated region (UTR) rare variants, (6) upstream region rare variants, (7)
195 downstream region rare variants of each protein-coding gene and (8) rare variants in
196 ncRNA genes²⁴. The promoter rare variants were defined as rare variants in the ± 3 -
197 kilobase (kb) window of transcription start sites with the overlap of CAGE sites or DHS
198 sites. The enhancer rare variants were defined as RVs in GeneHancer-predicted
199 regions with the overlap of CAGE sites or DHS sites. The UTR, upstream, downstream
200 and ncRNA rare variants were defined by GENCODE VEP categories³². With a well-
201 calibrated overall distribution of MultiSTAAR-O *P* values (**Extended Data Fig. 1d**) and
202 at a Bonferroni-corrected significance threshold of $\alpha = 0.05/(20,000 \times 7) = 3.57 \times$
203 10^{-7} , accounting for seven different noncoding masks across protein-coding genes,
204 MultiSTAAR-O identified 76 genome-wide significant associations using unconditional
205 multi-trait analysis (**Extended Data Fig. 1c, Supplementary Table 5**). After

206 conditioning on known lipids-associated variants^{26,38,39}, 6 out of the 76 associations
207 remained significant at the Bonferroni-corrected threshold of $\alpha = 0.05/76 = 6.58 \times$
208 10^{-4} (**Table 2**). These included promoter CAGE and enhancer CAGE rare variants in
209 *APOA1*, promoter DHS rare variants in *CETP*, enhancer CAGE rare variants in *SPC24*,
210 and enhancer DHS rare variants in *NIPSNAP3A* and *LIPC*.

211

212 MultiSTAAR-O further identified 6 genome-wide significant associations using
213 unconditional multi-trait analysis at $\alpha = 0.05/20,000 = 2.50 \times 10^{-6}$ accounting for
214 ncRNA genes (**Extended Data Fig. 1e, Supplementary Table 5**), with 3 rare variant
215 associations in *RP11-15F12.3*, *RP11-310H4.2* and *MIR4497* remained significant at
216 $\alpha = 0.05/6 = 8.33 \times 10^{-3}$ after conditioning on known lipids-associated variants^{26,38,39}
217 (**Table 2**).

218

219 Notably, among the 9 conditionally significant noncoding rare variants associations with
220 lipid traits, 4 of them were not detected by any of the three single-trait analysis (LDL-C,
221 HDL-C or TG) using unconditional analysis of STAAR-O, including the associations of
222 enhancer DHS rare variants in *NIPSNAP3A* and *LIPC* as well as ncRNA rare variants in
223 *RP11-310H4.2* and *MIR4497* (**Supplementary Table 5**). These results demonstrate
224 that MultiSTAAR-O can increase power over existing methods, and identify additional
225 trait-associated signals by leveraging cross-phenotype correlations between multiple
226 traits.

227

228 **Genetic region multi-trait analysis of rare variants**

229 We next applied MultiSTAAR-O to perform genetic region multi-trait analysis to identify
230 rare variants associated with lipid traits in TOPMed. Rare variants residing in 2-kilobase
231 (kb) sliding windows with a 1-kb skip length were aggregated and analyzed using a joint
232 model for LDL-C, HDL-C and TG. We incorporated 12 quantitative annotations,
233 including 9 aPCs, CADD, LINSIGHT, FATHMM-XF along with the two MAF weights in
234 MultiSTAAR-O (**Methods**). The overall distribution of MultiSTAAR-O *P* values was well-
235 calibrated for the multi-trait analysis (**Fig. 2b**). At a Bonferroni-corrected significance
236 threshold of $\alpha = 0.05 / (2.65 \times 10^6) = 1.89 \times 10^{-8}$ accounting for 2.65 million 2-kb
237 sliding windows across the genome, MultiSTAAR-O identified 502 genome-wide
238 significant associations using unconditional multi-trait analysis (**Fig. 2a, Supplementary**
239 **Table 6**). By dynamically incorporating multiple functional annotations capturing
240 different aspects of variant function, MultiSTAAR-O detected more significant sliding
241 windows and showed consistently smaller *P* values for top sliding windows compared
242 with multi-trait analysis using only MAFs as the weight (**Fig. 2c**). After conditioning on
243 known lipids-associated variants^{26,38,39}, 7 out of the 502 associations remained
244 significant at the Bonferroni-corrected threshold of $\alpha = 0.05 / 502 = 9.96 \times 10^{-5}$ (**Table**
245 **3**), including two sliding windows in *DOCK7* (chromosome 1: 62,651,447 - 62,653,446
246 bp; chromosome 1: 62,652,447 - 62,654,446 bp) and an intergenic sliding window
247 (chromosome 1: 145,530,447 - 145,532,446 bp) that were not detected by any of the
248 three single-trait analysis (LDL-C, HDL-C or TG) using STAAR-O (**Supplementary**
249 **Table 6**). Notably, all known lipids-associated variants indexed in the previous literature
250 were at least 1-Mb away from the intergenic sliding window.

251

252 **Comparison of MultiSTAAR-O with existing multi-trait rare variant tests**

253 Using TOPMed Freeze 8 WGS data, our gene-centric multi-trait analysis of coding rare
254 variants identified 34 conditionally significant associations with lipid traits (**Table 1**),
255 including *NPC1L1* and *SCARB1* missense rare variants that were missed by multi-trait
256 burden, SKAT and ACAT-V tests (**Supplementary Table 4**). Among the 9 and 7
257 conditionally significant associations detected in gene-centric multi-trait analysis of
258 noncoding rare variants and genetic region multi-trait analysis, MultiSTAAR-O identified
259 1 and 2 associations, respectively, that were missed by multi-trait burden, SKAT and
260 ACAT-V tests (**Supplementary Tables 5-6**). These associations included enhancer
261 CAGE rare variants in *SPC24* and two sliding windows in *LDLR* (chromosome 19:
262 11,104,367 - 11,106,366 bp; chromosome 19: 11,105,367 - 11,107,366 bp).

263

264 **Computation cost**

265 The computational cost for MultiSTAAR-O to perform WGS multi-trait rare variant
266 analysis of $n = 61,838$ related TOPMed lipids samples was 2 hours using 250 2.10-GHz
267 computing cores with 12-GB memory for gene-centric coding analysis; or 20 hours
268 using 250 2.10-GHz computing cores with 24-GB memory for gene-centric noncoding
269 analysis; 2 hours using 250 2.10-GHz computing cores with 12-GB memory of ncRNA
270 analysis; and 20 hours using 500 2.10-GHz computing cores with 24-GB memory for
271 sliding window analysis. Runtime for all analyses scales linearly with the sample size²⁴.

272

273 **Discussion**

274 In this study, we have introduced MultiSTAAR as a general statistical framework and a
275 flexible analytical pipeline for performing functionally-informed multi-trait RVAS in large-
276 scale WGS studies. MultiSTAAR improves power by analyzing multiple traits
277 simultaneously and dynamically incorporating multiple functional annotations, while
278 accounting for relatedness and population structure among study samples.

279

280 By jointly analyzing multiple quantitative traits using a multivariate linear mixed model,
281 MultiSTAAR explicitly leverages the correlation among multiple phenotypes to enhance
282 power for detecting additional association signals, outperforming single-trait analyses of
283 the individual phenotypes. MultiSTAAR also enables conditional multi-trait analysis to
284 identify putatively novel rare variant associations independent of a set of known
285 variants. Using TOPMed Freeze 8 WGS data, our gene-centric multi-trait analysis of
286 noncoding rare variants identified 9 conditionally significant associations with lipid traits
287 (**Table 2**), including 4 noncoding associations that were missed by single-trait analysis
288 using STAAR (**Supplementary Table 5**). Our genetic region multi-trait analysis of rare
289 variants identified 7 conditionally significant 2-kb sliding windows associated with lipid
290 traits (**Table 3**), including 3 associations that were missed by single-trait analysis using
291 STAAR (**Supplementary Table 6**).

292

293 By dynamically incorporating multiple annotations capturing diverse aspects of variant
294 biological function in the second step, MultiSTAAR further improves power over existing
295 multi-trait rare variant analysis methods. Our simulation studies demonstrated that
296 MultiSTAAR-O maintained accurate type I error rates while achieving considerable

297 power gains over multi-trait burden, SKAT and ACAT-V tests that do not incorporate
298 functional annotation information (**Extended Data Figs. 2-5, Supplementary Figs. 1-**
299 **4**). Notably, the existing ACAT-V method⁹ does not support multi-trait analysis. We
300 extended it to accommodate multi-trait settings and incorporated the multi-trait ACAT-V
301 test into the MultiSTAAR framework (**Methods**).

302
303 Implemented as a flexible analytical pipeline, MultiSTAAR allows for customized input
304 phenotype selection, variant set definition and user-specified annotation weights to
305 facilitate functionally-informed multi-trait analyses. In addition to rare variant association
306 analysis of coding and noncoding regions, MultiSTAAR also provides single-variant
307 multi-trait analysis for common and low-frequency variants under a given MAF or minor
308 allele count (MAC) cutoff (e.g. MAC ≥ 20). Using 61,838 TOPMed lipids samples, it took
309 8 hours using 250 2.10-GHz computing cores with 12-GB memory for single-variant
310 multi-trait analysis, which is scalable for large WGS/WES datasets. On the other hand,
311 MultiSTAAR could be further extended to allow for dynamic windows with data-adaptive
312 sizes in genetic region analysis^{24,44}, to properly leverage synthetic surrogates in the
313 presence of partially missing phenotypes⁴⁵, and to incorporate summary statistics for
314 meta-analysis of multiple WGS/WES studies⁴⁶.

315
316 In summary, MultiSTAAR provides a powerful statistical framework and a
317 computationally scalable analytical pipeline for large-scale WGS multi-trait analysis with
318 complex study samples. Compared to single-trait analysis, MultiSTAAR offers a notable
319 increase in statistical power when analyzing multiple moderately to highly correlated

320 traits, all while maintaining control over type I error rates across various genetic
321 architectures. As the sample sizes and number of available phenotypes increase in
322 biobank-scale sequencing studies, our proposed method may contribute to a better
323 understanding of the genetic architecture of complex traits by elucidating the role of rare
324 variants with pleiotropic effects.

325

326 **Acknowledgments**

327 This work was supported by grants R35-CA197449, U19-CA203654, U01-HG012064,
328 and U01-HG009088 (X. Lin), NHLBI TOPMed Fellowship (X. Li), R01-HL142711 and
329 R01-HL127564 (P.N. and G.M.P.), 75N92020D00001, HHSN268201500003I, N01-HC-
330 95159, 75N92020D00005, N01-HC-95160, 75N92020D00002, N01-HC-95161,
331 75N92020D00003, N01-HC-95162, 75N92020D00006, N01-HC-95163,
332 75N92020D00004, N01-HC-95164, 75N92020D00007, N01-HC-95165, N01-HC-95166,
333 N01-HC-95167, N01-HC-95168, N01-HC-95169, UL1-TR-000040, UL1-TR-001079,
334 UL1-TR-001420, UL1-TR001881, DK063491, R01-HL071051, R01-HL071205, R01-
335 HL071250, R01-HL071251, R01-HL071258, R01-HL071259, and UL1-RR033176
336 (J.I.R.), HHSN268201800001I and U01-HL137162 (K.M.R.), 1R35-HL135818, R01-
337 HL113338, and HL046389 (S.R.), HL105756 (B.M.P.), HHSN268201600018C,
338 HHSN268201600001C, HHSN268201600002C, HHSN268201600003C, and
339 HHSN268201600004C (C.K.), R01-MD012765 and R01-DK117445 (N.F.),
340 18CDA34110116 from American Heart Association (P.S.d.V.), R01-HL153805, R03-
341 HL154284 (B.E.C.), HHSN268201700001I, HHSN268201700002I,
342 HHSN268201700003I, HHSN268201700005I, and HHSN268201700004I (E.B.), U01-

343 HL072524, R01-HL104135-04S1, U01-HL054472, U01-HL054473, U01-HL054495,
344 U01-HL054509, and R01-HL055673-18S1 (D.K.A.), U01-HL72518, HL087698,
345 HL49762, HL59684, HL58625, HL071025, HL112064, NR0224103, and M01-
346 RR000052 (to the Johns Hopkins General Clinical Research Center). This work was
347 supported by R01 HL92301, R01 HL67348, R01 NS058700, R01 AR48797, R01
348 DK071891, R01 AG058921, the General Clinical Research Center of the Wake Forest
349 University School of Medicine (M01 RR07122, F32 HL085989), the American Diabetes
350 Association, and a pilot grant from the Claude Pepper Older Americans Independence
351 Center of Wake Forest University Health Sciences (P60 AG10484). The Framingham
352 Heart Study (FHS) acknowledges the support of contracts NO1-HC-25195,
353 HHSN268201500001I and 75N92019D00031 from the National Heart, Lung and Blood
354 Institute and grant supplement R01 HL092577-06S1 for this research. We also
355 acknowledge the dedication of the FHS study participants without whom this research
356 would not be possible. R.S.V. is supported in part by the Evans Medical Foundation and
357 the Jay and Louis Coffman Endowment from the Department of Medicine, Boston
358 University School of Medicine. The Jackson Heart Study (JHS) is supported and
359 conducted in collaboration with Jackson State University (HHSN268201800013I),
360 Tougaloo College (HHSN268201800014I), the Mississippi State Department of Health
361 (HHSN268201800015I) and the University of Mississippi Medical Center
362 (HHSN268201800010I, HHSN268201800011I and HHSN268201800012I) contracts
363 from the National Heart, Lung, and Blood Institute (NHLBI) and the National Institute on
364 Minority Health and Health Disparities (NIMHD). The authors also wish to thank the
365 staffs and participants of the JHS. Support for GENOA was provided by the National

366 Heart, Lung and Blood Institute (U01HL054457, U01HL054464, U01HL054481,
367 R01HL119443, and R01HL087660) of the National Institutes of Health. Collection of the
368 San Antonio Family Study data was supported in part by National Institutes of Health
369 (NIH) grants P01 HL045522, MH078143, MH078111 and MH083824; and whole
370 genome sequencing of SAFS subjects was supported by U01 DK085524 and R01
371 HL113323. Molecular data for the Trans-Omics in Precision Medicine (TOPMed)
372 program was supported by the National Heart, Lung and Blood Institute (NHLBI). Core
373 support including centralized genomic read mapping and genotype calling, along with
374 variant quality metrics and filtering were provided by the TOPMed Informatics Research
375 Center (3R01HL-117626-02S1; contract HHSN268201800002I). Core support including
376 phenotype harmonization, data management, sample-identity QC, and general program
377 coordination were provided by the TOPMed Data Coordinating Center (R01HL-120393;
378 U01HL-120393; contract HHSN268201800001I). We gratefully acknowledge the studies
379 and participants who provided biological samples and data for TOPMed. The full study
380 specific acknowledgements are detailed in **Supplementary Note**.

381

382 **Author contributions**

383 X. Li, H.C., Z. Li, Z. Liu and X. Lin designed the experiments. X. Li, H.C., Z. Li and X.
384 Lin performed the experiments. X. Li, H.C., M.S.S., E.V.B., Y.W., R.S., Z.R.M., Z.Y.,
385 D.K.A., J.C.B., J.B., E.B., D.W.B., J.A.B., B.E.C., A.P.C., J.C.C., N.C., Y.D.I.C., J.E.C.,
386 P.S.d.V., M.F., N.F., B.I.F., C.G., N.L.H.C., J.H., L.H., Y.J.H., M.R.I., R.C.K., S.L.R.K.,
387 T.K., I.K., C.K., B.G.K., C.L., R.J.F.L., M.C.M., L.W.M., R.A.M., R.L.M., B.D.M., M.E.M.,
388 A.C.M., N.D.P., P.A.P., B.M.P., L.M.R., S.R., A.P.R., S.S.R., C.M.S., J.A.S., K.D.T.,

389 H.T., R.S.V., Z.W., L.R.Y., B.Y., K.M.R., J.I.R., G.M.P., P.N., Z. Li, Z. Liu and X. Lin
390 acquired, analyzed or interpreted data. G.M.P., P.N. and the NHLBI TOPMed Lipids
391 Working Group provided administrative, technical or material support. X. Li, Z. Li, Z. Liu
392 and X. Lin drafted the manuscript and revised it according to suggestions by the
393 coauthors. All authors critically reviewed the manuscript, suggested revisions as needed
394 and approved the final version.

395

396 **Competing interests**

397 Z.R.M. is an employee of Insitro. M.E.M. receives research funding from Regeneron
398 Pharmaceutical Inc., unrelated to this project. B.M.P. serves on the Steering Committee
399 of the Yale Open Data Access Project funded by Johnson & Johnson. L.M.R. is a
400 consultant for the TOPMed Administrative Coordinating Center (via Westat). X. Lin is a
401 consultant of AbbVie Pharmaceuticals and Verily Life Sciences. The remaining authors
402 declare no competing interests.

403

404 **NHLBI Trans-Omics for Precision Medicine (TOPMed) Consortium**

405 Namiko Abe⁵⁰, Gonçalo Abecasis⁵¹, Francois Aguet⁵², Christine Albert⁵³, Laura
406 Almasy⁵⁴, Alvaro Alonso⁵⁵, Seth Ament⁵⁶, Peter Anderson⁵⁷, Pramod Anugu⁵⁸, Deborah
407 Applebaum-Bowden⁵⁹, Kristin Ardlie⁵², Dan Arking⁶⁰, Allison Ashley-Koch⁶¹, Stella
408 Aslibekyan⁶², Tim Assimes⁶³, Paul Auer⁶⁴, Dimitrios Avramopoulos⁶⁰, Najib Ayas⁶⁵,
409 Adithya Balasubramanian⁶⁶, John Barnard⁶⁷, Kathleen Barnes⁶⁸, R. Graham Barr⁶⁹,
410 Emily Barron-Casella⁶⁰, Lucas Barwick⁷⁰, Terri Beaty⁶⁰, Gerald Beck⁷¹, Diane Becker⁷²,
411 Lewis Becker⁶⁰, Rebecca Beer⁷³, Amber Beitelhees⁵⁶, Emelia Benjamin⁷⁴, Takis

412 Benos⁷⁵, Marcos Bezerra⁷⁶, Larry Bielak⁵¹, Thomas Blackwell⁵¹, Nathan Blue⁷⁷, Russell
413 Bowler⁷⁸, Ulrich Broeckel⁷⁹, Jai Broome⁵⁷, Deborah Brown⁸⁰, Karen Bunting⁵⁰, Esteban
414 Burchard⁸¹, Carlos Bustamante⁸², Erin Buth⁸³, Jonathan Cardwell⁸⁴, Vincent Carey⁸⁵,
415 Julie Carrier⁸⁶, Cara Carty⁸⁷, Richard Casaburi⁸⁸, Juan P Casas Romero⁸⁹, James
416 Casella⁶⁰, Peter Castaldi⁹⁰, Mark Chaffin⁵², Christy Chang⁵⁶, Yi-Cheng Chang⁹¹, Daniel
417 Chasman⁹², Sameer Chavan⁸⁴, Bo-Juen Chen⁵⁰, Wei-Min Chen⁹³, Michael Cho⁸⁵,
418 Seung Hoan Choi⁵², Lee-Ming Chuang⁹⁴, Mina Chung⁹⁵, Ren-Hua Chung⁹⁶, Clary
419 Clish⁹⁷, Suzy Comhair⁹⁸, Matthew Conomos⁸³, Elaine Cornell⁹⁹, Adolfo Correa¹⁰⁰,
420 Carolyn Crandall⁸⁸, James Crapo¹⁰¹, L. Adrienne Cupples¹⁰², Jeffrey Curtis¹⁰³, Brian
421 Custer¹⁰⁴, Coleen Damcott⁵⁶, Dawood Darbar¹⁰⁵, Sean David¹⁰⁶, Colleen Davis⁵⁷,
422 Michelle Daya⁸⁴, Michael DeBaun¹⁰⁷, Dawn DeMeo⁸⁵, Ranjan Deka¹⁰⁸, Scott Devine⁵⁶,
423 Huyen Dinh⁶⁶, Harsha Doddapaneni¹⁰⁹, Qing Duan¹¹⁰, Shannon Dugan-Perez¹¹¹, Ravi
424 Duggirala¹¹², Jon Peter Durda¹¹³, Susan K. Dutcher¹¹⁴, Charles Eaton¹¹⁵, Lynette
425 Ekunwe⁵⁸, Adel El Boueiz¹¹⁶, Patrick Ellinor¹¹⁷, Leslie Emery⁵⁷, Serpil Erzurum¹¹⁸,
426 Charles Farber⁹³, Jesse Farek⁶⁶, Tasha Fingerlin¹¹⁹, Matthew Flickinger⁵¹, Chris
427 Frazar⁵⁷, Mao Fu⁵⁶, Stephanie M. Fullerton⁵⁷, Lucinda Fulton¹²⁰, Stacey Gabriel⁵²,
428 Weiniu Gan⁷³, Shanshan Gao⁸⁴, Yan Gao⁵⁸, Margery Gass¹²¹, Heather Geiger¹²², Bruce
429 Gelb¹²³, Mark Geraci¹²⁴, Soren Germer⁵⁰, Robert Gerszten¹²⁵, Auyon Ghosh⁸⁵, Richard
430 Gibbs⁶⁶, Chris Gignoux⁶³, Mark Gladwin¹²⁶, David Glahn¹²⁷, Stephanie Gogarten⁵⁷, Da-
431 Wei Gong⁵⁶, Harald Goring¹²⁸, Sharon Graw¹²⁹, Kathryn J. Gray¹³⁰, Daniel Grine⁸⁴, Colin
432 Gross⁵¹, Yue Guan⁵⁶, Xiuqing Guo¹³¹, Namrata Gupta¹³², Jeff Haessler¹²¹, Michael
433 Hall¹³³, Yi Han⁶⁶, Patrick Hanly¹³⁴, Daniel Harris¹³⁵, Nicola L. Hawley¹³⁶, Ben Heavner⁸³,
434 Susan Heckbert¹³⁷, Ryan Hernandez⁸¹, David Herrington¹³⁸, Craig Hersh¹³⁹, Bertha

435 Hidalgo⁶², James Hixson¹⁴⁰, Brian Hobbs¹⁴¹, John Hokanson⁸⁴, Elliott Hong⁵⁶, Karin
436 Hoth¹⁴², Chao (Agnes) Hsiung¹⁴³, Jianhong Hu⁶⁶, Haley Huston¹⁴⁴, Chii Min Hwu¹⁴⁵,
437 Rebecca Jackson¹⁴⁶, Deepti Jain⁵⁷, Cashell Jaquish¹⁴⁷, Jill Johnsen¹⁴⁸, Andrew
438 Johnson⁷³, Craig Johnson⁵⁷, Rich Johnston⁵⁵, Kimberly Jones⁶⁰, Hyun Min Kang¹⁴⁹,
439 Shannon Kelly¹⁵⁰, Eimear Kenny¹²³, Michael Kessler⁵⁶, Alyna Khan⁵⁷, Ziad Khan⁶⁶,
440 Wonji Kim¹⁵¹, John Kimoff¹⁵², Greg Kinney¹⁵³, Barbara Konkle¹⁵⁴, Holly Kramer¹⁵⁵,
441 Christoph Lange¹⁵⁶, Ethan Lange⁸⁴, Leslie Lange¹⁵⁷, Cathy Laurie⁵⁷, Cecelia Laurie⁵⁷,
442 Meryl LeBoff⁸⁵, Jonathon LeFaive⁵¹, Jiwon Lee⁸⁵, Sandra Lee⁶⁶, Wen-Jane Lee¹⁴⁵,
443 David Levine⁵⁷, Daniel Levy⁷³, Joshua Lewis⁵⁶, Xiaohui Li¹³¹, Yun Li¹¹⁰, Henry Lin¹³¹,
444 Honghuang Lin¹⁵⁸, Simin Liu¹⁵⁹, Yongmei Liu¹⁶⁰, Yu Liu¹⁶¹, Steven Lubitz¹¹⁷, Kathryn
445 Lunetta¹⁶², James Luo⁷³, Ulysses Magalang¹⁶³, Barry Make⁶⁰, Ani Manichaikul⁹³, Alisa
446 Manning¹⁶⁴, JoAnn Manson⁸⁵, Melissa Marton¹²², Susan Mathai⁸⁴, Susanne May⁸³,
447 Patrick McArdle⁵⁶, Merry-Lynn McDonald¹⁶⁵, Sean McFarland¹⁵¹, Stephen McGarvey¹⁶⁶,
448 Daniel McGoldrick¹⁶⁷, Caitlin McHugh⁸³, Becky McNeil¹⁶⁸, Hao Mei⁵⁸, James Meigs¹⁶⁹,
449 Vipin Menon⁶⁶, Luisa Mestroni¹²⁹, Ginger Metcalf⁶⁶, Deborah A Meyers¹⁷⁰, Emmanuel
450 Mignot¹⁷¹, Julie Mikulla⁷³, Nancy Min⁵⁸, Mollie Minear¹⁷², Matt Moll⁹⁰, Zeineen Momin⁶⁶,
451 Courtney Montgomery¹⁷³, Donna Muzny⁶⁶, Josyf C Mychaleckyj⁹³, Girish Nadkarni¹²³,
452 Rakhi Naik⁶⁰, Take Naseri¹⁷⁴, Sergei Nekhai¹⁷⁵, Sarah C. Nelson⁸³, Bonnie Neltner⁸⁴,
453 Caitlin Nessner⁶⁶, Deborah Nickerson¹⁷⁶, Osuji Nkechinyere⁶⁶, Kari North¹¹⁰, Jeff
454 O'Connell¹⁷⁷, Tim O'Connor⁵⁶, Heather Ochs-Balcom¹⁷⁸, Geoffrey Okwuonu⁶⁶, Allan
455 Pack¹⁷⁹, David T. Paik¹⁸⁰, James Pankow¹⁸¹, George Papanicolaou⁷³, Cora Parker¹⁸²,
456 Juan Manuel Peralta¹¹², Marco Perez⁶³, James Perry⁵⁶, Ulrike Peters¹⁸³, Lawrence S
457 Phillips⁵⁵, Jacob Pleiness⁵¹, Toni Pollin⁵⁶, Wendy Post¹⁸⁴, Julia Powers Becker¹⁸⁵,

458 Meher Preethi Boorgula⁸⁴, Michael Preuss¹²³, Pankaj Qasba⁷³, Dandi Qiao⁸⁵, Zhaohei
459 Qin⁵⁵, Nicholas Rafaels¹⁸⁶, Mahitha Rajendran⁶⁶, D.C. Rao¹²⁰, Laura Rasmussen-
460 Torvik¹⁸⁷, Aakrosh Ratan⁹³, Robert Reed⁵⁶, Catherine Reeves¹⁸⁸, Elizabeth Regan¹⁸⁹,
461 Muagututi'a Sefuiva Reupena¹⁹⁰, Rebecca Robillard¹⁹¹, Nicolas Robine¹²², Dan
462 Roden¹⁹², Carolina Roselli⁵², Ingo Ruczinski⁶⁰, Alexi Runnels¹²², Pamela Russell⁸⁴,
463 Sarah Ruuska¹⁹³, Kathleen Ryan⁵⁶, Ester Cerdeira Sabino¹⁹⁴, Danish Saleheen¹⁹⁵,
464 Shabnam Salimi¹⁹⁶, Sejal Salvi⁶⁶, Steven Salzberg⁶⁰, Kevin Sandow¹⁹⁷, Vijay G.
465 Sankaran¹⁹⁸, Jireh Santibanez⁶⁶, Karen Schwander¹²⁰, David Schwartz⁸⁴, Frank
466 Sciurba¹²⁶, Christine Seidman¹⁹⁹, Jonathan Seidman²⁰⁰, Vivien Sheehan²⁰¹, Stephanie
467 L. Sherman²⁰², Amol Shetty⁵⁶, Aniket Shetty⁸⁴, Wayne Hui-Heng Sheu¹⁴⁵, M. Benjamin
468 Shoemaker²⁰³, Brian Silver²⁰⁴, Edwin Silverman⁸⁵, Robert Skomro²⁰⁵, Albert Vernon
469 Smith²⁰⁶, Josh Smith⁵⁷, Nicholas Smith²⁰⁷, Tanja Smith⁵⁰, Sylvia Smoller²⁰⁸, Beverly
470 Snively²⁰⁹, Michael Snyder²¹⁰, Tamar Sofer¹²⁵, Nona Sotoodehnia⁵⁷, Adrienne M. Stilp⁵⁷,
471 Garrett Storm²¹¹, Elizabeth Streeten⁵⁶, Jessica Lasky Su²¹², Yun Ju Sung¹²⁰, Jody
472 Sylvia⁸⁵, Adam Szpiro⁵⁷, Frédéric Séries²¹³, Daniel Taliun⁵¹, Hua Tang²¹⁰, Margaret
473 Taub⁶⁰, Matthew Taylor¹²⁹, Simeon Taylor⁵⁶, Marilyn Telen⁶¹, Timothy A. Thornton⁵⁷,
474 Machiko Threlkeld²¹⁴, Lesley Tinker²¹⁵, David Tirschwell⁵⁷, Sarah Tishkoff²¹⁶, Catherine
475 Tong²¹⁷, Russell Tracy²¹⁸, Michael Tsai¹⁸¹, Dhananjay Vaidya⁶⁰, David Van Den Berg²¹⁹,
476 Peter VandeHaar⁵¹, Scott Vrieze¹⁸¹, Tarik Walker⁸⁴, Robert Wallace¹⁴², Avram Walts⁸⁴,
477 Fei Fei Wang⁵⁷, Heming Wang²²⁰, Jiongming Wang²²¹, Karol Watson⁸⁸, Jennifer Watt⁶⁶,
478 Daniel E. Weeks²²², Joshua Weinstock¹⁴⁹, Bruce Weir⁵⁷, Scott T Weiss²²³, Lu-Chen
479 Weng¹¹⁷, Jennifer Wessel²²⁴, Cristen Willer¹⁰³, Kayleen Williams⁸³, L. Keoki Williams²²⁵,
480 Scott Williams²²⁶, Carla Wilson⁸⁵, James Wilson²²⁷, Lara Winterkorn¹²², Quenna

481 Wong⁵⁷, Baojun Wu²²⁸, Joseph Wu¹⁸⁰, Huichun Xu⁵⁶, Ivana Yang⁸⁴, Ketian Yu⁵¹,
482 Seyedeh Maryam Zekavat⁵², Yingze Zhang²²⁹, Snow Xueyan Zhao¹⁰¹, Wei Zhao²³⁰,
483 Xiaofeng Zhu²³¹, Elad Ziv²³², Michael Zody⁵⁰, Sebastian Zoellner⁵¹, Mariza de
484 Andrade²³³, Lisa de las Fuentes²³⁴
485
486 50 - New York Genome Center, New York, New York, 10013, US; 51 - University of
487 Michigan, Ann Arbor, Michigan, 48109, US; 52 - Broad Institute, Cambridge,
488 Massachusetts, 2142, US; 53 - Cedars Sinai, Boston, Massachusetts, 2114, US; 54 -
489 Children's Hospital of Philadelphia, University of Pennsylvania, Philadelphia,
490 Pennsylvania, 19104, US; 55 - Emory University, Atlanta, Georgia, 30322, US; 56 -
491 University of Maryland, Baltimore, Maryland, 21201, US; 57 - University of Washington,
492 Seattle, Washington, 98195, US; 58 - University of Mississippi, Jackson, Mississippi,
493 38677, US; 59 - National Institutes of Health, Bethesda, Maryland, 20892, US; 60 -
494 Johns Hopkins University, Baltimore, Maryland, 21218, US; 61 - Duke University,
495 Durham, North Carolina, 27708, US; 62 - University of Alabama, Birmingham, Alabama,
496 35487, US; 63 - Stanford University, Stanford, California, 94305, US; 64 - Medical
497 College of Wisconsin, Milwaukee, Wisconsin, 53211, US; 65 - Providence Health Care,
498 Medicine, Vancouver, CA; 66 - Baylor College of Medicine Human Genome Sequencing
499 Center, Houston, Texas, 77030, US; 67 - Cleveland Clinic, Cleveland, Ohio, 44195, US;
500 68 - Tempus, University of Colorado Anschutz Medical Campus, Aurora, Colorado,
501 80045, US; 69 - Columbia University, New York, New York, 10032, US; 70 - The
502 Emmes Corporation, LTRC, Rockville, Maryland, 20850, US; 71 - Cleveland Clinic,
503 Quantitative Health Sciences, Cleveland, Ohio, 44195, US; 72 - Johns Hopkins

504 University, Medicine, Baltimore, Maryland, 21218, US; 73 - National Heart, Lung, and
505 Blood Institute, National Institutes of Health, Bethesda, Maryland, 20892, US; 74 -
506 Boston University, Massachusetts General Hospital, Boston University School of
507 Medicine, Boston, Massachusetts, 2114, US; 75 - University of Florida, Epidemiology,
508 Gainesville, Florida, 32610, US; 76 - Fundação de Hematologia e Hemoterapia de
509 Pernambuco - Hemope, Recife, 52011-000, BR; 77 - University of Utah, Obstetrics and
510 Gynecology, Salt Lake City, Utah, 84132, US; 78 - National Jewish Health, National
511 Jewish Health, Denver, Colorado, 80206, US; 79 - Medical College of Wisconsin,
512 Pediatrics, Milwaukee, Wisconsin, 53226, US; 80 - University of Texas Health at
513 Houston, Pediatrics, Houston, Texas, 77030, US; 81 - University of California, San
514 Francisco, San Francisco, California, 94143, US; 82 - Stanford University, Biomedical
515 Data Science, Stanford, California, 94305, US; 83 - University of Washington,
516 Biostatistics, Seattle, Washington, 98195, US; 84 - University of Colorado at Denver,
517 Denver, Colorado, 80204, US; 85 - Brigham & Women's Hospital, Boston,
518 Massachusetts, 2115, US; 86 - University of Montreal, US; 87 - Washington State
519 University, Pullman, Washington, 99164, US; 88 - University of California, Los Angeles,
520 Los Angeles, California, 90095, US; 89 - Brigham & Women's Hospital, US; 90 -
521 Brigham & Women's Hospital, Medicine, Boston, Massachusetts, 2115, US; 91 -
522 National Taiwan University, Taipei, 10617, TW; 92 - Brigham & Women's Hospital,
523 Division of Preventive Medicine, Boston, Massachusetts, 2215, US; 93 - University of
524 Virginia, Charlottesville, Virginia, 22903, US; 94 - National Taiwan University, National
525 Taiwan University Hospital, Taipei, 10617, TW; 95 - Cleveland Clinic, Cleveland Clinic,
526 Cleveland, Ohio, 44195, US; 96 - National Health Research Institute Taiwan, Miaoli

527 County, 350, TW; 97 - Broad Institute, Metabolomics Platform, Cambridge,
528 Massachusetts, 2142, US; 98 - Cleveland Clinic, Immunity and Immunology, Cleveland,
529 Ohio, 44195, US; 99 - University of Vermont, Burlington, Vermont, 5405, US; 100 -
530 University of Mississippi, Population Health Science, Jackson, Mississippi, 39216, US;
531 101 - National Jewish Health, Denver, Colorado, 80206, US; 102 - Boston University,
532 Biostatistics, Boston, Massachusetts, 2115, US; 103 - University of Michigan, Internal
533 Medicine, Ann Arbor, Michigan, 48109, US; 104 - Vitalant Research Institute, San
534 Francisco, California, 94118, US; 105 - University of Illinois at Chicago, Chicago, Illinois,
535 60607, US; 106 - University of Chicago, Chicago, Illinois, 60637, US; 107 - Vanderbilt
536 University, Nashville, Tennessee, 37235, US; 108 - University of Cincinnati, Cincinnati,
537 Ohio, 45220, US; 109 - Baylor College of Medicine Human Genome Sequencing
538 Center, Houston, Texas, 77030; 110 - University of North Carolina, Chapel Hill, North
539 Carolina, 27599, US; 111 - Baylor College of Medicine Human Genome Sequencing
540 Center, BCM, Houston, Texas, 77030, US; 112 - University of Texas Rio Grande Valley
541 School of Medicine, Edinburg, Texas, 78539, US; 113 - University of Vermont,
542 Pathology and Laboratory Medicine, Burlington, Vermont, 5405, US; 114 - Washington
543 University in St Louis, Genetics, St Louis, Missouri, 63110, US; 115 - Brown University,
544 Providence, Rhode Island, 2912, US; 116 - Harvard University, Channing Division of
545 Network Medicine, Cambridge, Massachusetts, 2138, US; 117 - Massachusetts General
546 Hospital, Boston, Massachusetts, 2114, US; 118 - Cleveland Clinic, Lerner Research
547 Institute, Cleveland, Ohio, 44195, US; 119 - National Jewish Health, Center for Genes,
548 Environment and Health, Denver, Colorado, 80206, US; 120 - Washington University in
549 St Louis, St Louis, Missouri, 63130, US; 121 - Fred Hutchinson Cancer Research

550 Center, Seattle, Washington, 98109, US; 122 - New York Genome Center, New York
551 City, New York, 10013, US; 123 - Icahn School of Medicine at Mount Sinai, New York,
552 New York, 10029, US; 124 - University of Pittsburgh, Pittsburgh, Pennsylvania, US; 125
553 - Beth Israel Deaconess Medical Center, Boston, Massachusetts, 2215, US; 126 -
554 University of Pittsburgh, Pittsburgh, Pennsylvania, 15260, US; 127 - Boston Children's
555 Hospital, Harvard Medical School, Department of Psychiatry, Boston, Massachusetts,
556 2115, US; 128 - University of Texas Rio Grande Valley School of Medicine, San
557 Antonio, Texas, 78229, US; 129 - University of Colorado Anschutz Medical Campus,
558 Aurora, Colorado, 80045, US; 130 - Mass General Brigham, Obstetrics and
559 Gynecology, Boston, Massachusetts, 2115, US; 131 - Lundquist Institute, Torrance,
560 California, 90502, US; 132 - Broad Institute, Broad Institute, Cambridge,
561 Massachusetts, 2142, US; 133 - University of Mississippi, Cardiology, Jackson,
562 Mississippi, 39216, US; 134 - University of Calgary, Medicine, Calgary, CA; 135 -
563 University of Maryland, Genetics, Philadelphia, Pennsylvania, 19104, US; 136 - Yale
564 University, Department of Chronic Disease Epidemiology, New Haven, Connecticut,
565 6520, US; 137 - University of Washington, Epidemiology, Seattle, Washington, 98195-
566 9458, US; 138 - Wake Forest Baptist Health, Winston-Salem, North Carolina, 27157,
567 US; 139 - Brigham & Women's Hospital, Channing Division of Network Medicine,
568 Boston, Massachusetts, 2115, US; 140 - University of Texas Health at Houston,
569 Houston, Texas, 77225, US; 141 - Regeneron Genetics Center, Boston,
570 Massachusetts, 2115, US; 142 - University of Iowa, Iowa City, Iowa, 52242, US; 143 -
571 National Health Research Institute Taiwan, Institute of Population Health Sciences,
572 NHRI, Miaoli County, 350, TW; 144 - Blood Works Northwest, Seattle, Washington,

573 98104, US; 145 - Taichung Veterans General Hospital Taiwan, Taichung City, 407, TW;
574 146 - Oklahoma State University Medical Center, Internal Medicine, Division of
575 Endocrinology, Diabetes and Metabolism, Columbus, Ohio, 43210, US; 147 - National
576 Heart, Lung, and Blood Institute, National Institutes of Health, NHLBI, Bethesda,
577 Maryland, 20892, US; 148 - University of Washington, Medicine, Seattle, Washington,
578 98109, US; 149 - University of Michigan, Biostatistics, Ann Arbor, Michigan, 48109, US;
579 150 - University of California, San Francisco, San Francisco, California, 94118, US; 151
580 - Harvard University, Cambridge, Massachusetts, 2138, US; 152 - McGill University,
581 Montréal, QC H3A 0G4, CA; 153 - University of Colorado at Denver, Epidemiology,
582 Aurora, Colorado, 80045, US; 154 - Blood Works Northwest, Medicine, Seattle,
583 Washington, 98104, US; 155 - Loyola University, Public Health Sciences, Maywood,
584 Illinois, 60153, US; 156 - Harvard School of Public Health, Biostats, Boston,
585 Massachusetts, 2115, US; 157 - University of Colorado at Denver, Medicine, Aurora,
586 Colorado, 80048, US; 158 - Boston University, University of Massachusetts Chan
587 Medical School, Worcester, Massachusetts, 1655, US; 159 - Brown University,
588 Epidemiology and Medicine, Providence, Rhode Island, 2912, US; 160 - Duke
589 University, Cardiology, Durham, North Carolina, 27708, US; 161 - Stanford University,
590 Cardiovascular Institute, Stanford, California, 94305, US; 162 - Boston University,
591 Boston, Massachusetts, 2215, US; 163 - The Ohio State University, Division of
592 Pulmonary, Critical Care and Sleep Medicine, Columbus, Ohio, 43210, US; 164 - Broad
593 Institute, Harvard University, Massachusetts General Hospital; 165 - University of
594 Alabama, University of Alabama at Birmingham, Birmingham, Alabama, 35487, US; 166
595 - Brown University, Epidemiology, Providence, Rhode Island, 2912, US; 167 - University

596 of Washington, Genome Sciences, Seattle, Washington, 98195, US; 168 - RTI
597 International, US; 169 - Massachusetts General Hospital, Medicine, Boston,
598 Massachusetts, 2114, US; 170 - University of Arizona, Tucson, Arizona, 85721, US; 171
599 - Stanford University, Center For Sleep Sciences and Medicine, Palo Alto, California,
600 94304, US; 172 - National Institute of Child Health and Human Development, National
601 Institutes of Health, Bethesda, Maryland, 20892, US; 173 - Oklahoma Medical Research
602 Foundation, Genes and Human Disease, Oklahoma City, Oklahoma, 73104, US; 174 -
603 Ministry of Health, Government of Samoa, Apia, WS; 175 - Howard University,
604 Washington, District of Columbia, 20059, US; 176 - University of Washington,
605 Department of Genome Sciences, Seattle, Washington, 98195, US; 177 - University of
606 Maryland, Baltimore, Maryland, 21201, US; 178 - University at Buffalo, Buffalo, New
607 York, 14260, US; 179 - University of Pennsylvania, Division of Sleep
608 Medicine/Department of Medicine, Philadelphia, Pennsylvania, 19104-3403, US; 180 -
609 Stanford University, Stanford Cardiovascular Institute, Stanford, California, 94305, US;
610 181 - University of Minnesota, Minneapolis, Minnesota, 55455, US; 182 - RTI
611 International, Biostatistics and Epidemiology Division, Research Triangle Park, North
612 Carolina, 27709-2194, US; 183 - Fred Hutchinson Cancer Research Center, Fred Hutch
613 and UW, Seattle, Washington, 98109, US; 184 - Johns Hopkins University,
614 Cardiology/Medicine, Baltimore, Maryland, 21218, US; 185 - University of Colorado at
615 Denver, Medicine, Denver, Colorado, 80204, US; 186 - University of Colorado at
616 Denver, CCPM, Denver, Colorado, 80045, US; 187 - Northwestern University, Chicago,
617 Illinois, 60208, US; 188 - New York Genome Center, New York Genome Center, New
618 York City, New York, 10013, US; 189 - National Jewish Health, Medicine, Denver,

619 Colorado, 80206, US; 190 - Lutia I Puava Ae Mapu I Fagalele, Apia, WS; 191 -
620 University of Ottawa, Sleep Research Unit, University of Ottawa Institute for Mental
621 Health Research, Ottawa, ON K1Z 7K4, CA; 192 - Vanderbilt University, Medicine,
622 Pharmacology, Biomedicla Informatics, Nashville, Tennessee, 37235, US; 193 -
623 University of Washington, Seattle, Washington, 98104, US; 194 - Universidade de Sao
624 Paulo, Faculdade de Medicina, Sao Paulo, 1310000, BR; 195 - Columbia University,
625 New York, New York, 10027, US; 196 - University of Maryland, Pathology, Seattle,
626 Washington, 98195, US; 197 - Lundquist Institute, TGPS, Torrance, California, 90502,
627 US; 198 - Harvard University, Division of Hematology/Oncology, Boston,
628 Massachusetts, 2115, US; 199 - Harvard Medical School, Genetics, Boston,
629 Massachusetts, 2115, US; 200 - Harvard Medical School, Boston, Massachusetts,
630 2115, US; 201 - Emory University, Pediatrics, Atlanta, Georgia, 30307, US; 202 - Emory
631 University, Human Genetics, Atlanta, Georgia, 30322, US; 203 - Vanderbilt University,
632 Medicine/Cardiology, Nashville, Tennessee, 37235, US; 204 - UMass Memorial Medical
633 Center, Worcester, Massachusetts, 1655, US; 205 - University of Saskatchewan,
634 Saskatoon, SK S7N 5C9, CA; 206 - University of Michigan; 207 - University of
635 Washington, Epidemiology, Seattle, Washington, 98195, US; 208 - Albert Einstein
636 College of Medicine, New York, New York, 10461, US; 209 - Wake Forest Baptist
637 Health, Biostatistical Sciences, Winston-Salem, North Carolina, 27157, US; 210 -
638 Stanford University, Genetics, Stanford, California, 94305, US; 211 - University of
639 Colorado at Denver, Genomic Cardiology, Aurora, Colorado, 80045, US; 212 - Brigham
640 & Women's Hospital, Channing Department of Medicine, Boston, Massachusetts, 2115,
641 US; 213 - Université Laval, Quebec City, G1V 0A6, CA; 214 - University of Washington,

642 University of Washington, Department of Genome Sciences, Seattle, Washington,
643 98195, US; 215 - Fred Hutchinson Cancer Research Center, Cancer Prevention
644 Division of Public Health Sciences, Seattle, Washington, 98109, US; 216 - University of
645 Pennsylvania, Genetics, Philadelphia, Pennsylvania, 19104, US; 217 - University of
646 Washington, Department of Biostatistics, Seattle, Washington, 98195, US; 218 -
647 University of Vermont, Pathology & Laboratory Medicine, Burlington, Vermont, 5405,
648 US; 219 - University of Southern California, USC Methylation Characterization Center,
649 University of Southern California, California, 90033, US; 220 - Brigham & Women's
650 Hospital, Mass General Brigham, Boston, Massachusetts, 2115, US; 221 - University of
651 Michigan, US; 222 - University of Pittsburgh, Department of Human Genetics,
652 Pittsburgh, Pennsylvania, 15260, US; 223 - Brigham & Women's Hospital, Channing
653 Division of Network Medicine, Department of Medicine, Boston, Massachusetts, 2115,
654 US; 224 - Indiana University, Epidemiology, Indianapolis, Indiana, 46202, US; 225 -
655 Henry Ford Health System, Detroit, Michigan, 48202, US; 226 - Case Western Reserve
656 University; 227 - Beth Israel Deaconess Medical Center, Cardiology, Cambridge,
657 Massachusetts, 2139, US; 228 - Henry Ford Health System, Department of Medicine,
658 Detroit, Michigan, 48202, US; 229 - University of Pittsburgh, Medicine, Pittsburgh,
659 Pennsylvania, 15260, US; 230 - University of Michigan, Department of Epidemiology,
660 Ann Arbor, Michigan, 48109, US; 231 - Case Western Reserve University, Department
661 of Population and Quantitative Health Sciences, Cleveland, Ohio, 44106, US; 232 -
662 University of California, San Francisco, Medicine, San Francisco, California, 94143, US;
663 233 - Mayo Clinic, Health Quantitative Sciences Research, Rochester, Minnesota,

664 55905, US; 234 - Washington University in St Louis, Department of Medicine,

665 Cardiovascular Division, St. Louis, Missouri, 63110, US

666

667

668

669

670

671

672

673

674

675

676

677

678

679

680

681

682

683

684

685

686

687 **TABLES**

688 **Table 1 | TOPMed Gene-centric coding multi-trait analysis results of both**
689 **unconditional analysis and analysis conditional on known lipids-associated**
690 **variants.** A total of 61,838 samples from the TOPMed Program were considered in the
691 analysis. Results for the conditionally significant genes (unconditional MultiSTAAR-O
692 $P < 5.00 \times 10^{-7}$; conditional MultiSTAAR-O $P < 9.80 \times 10^{-4}$) are presented in the
693 table. MultiSTAAR-O is a two-sided test. Chr. no., chromosome number; Category,
694 functional category; No. of SNVs, number of rare variants (MAF < 1%) of the particular
695 coding functional category in the gene; MultiSTAAR-O, MultiSTAAR-O P value; Variants
696 (adjusted), adjusted variants in the conditional analysis.

697

Gene	Chr. no.	Category	No. of SNVs	MultiSTAAR-O (Unconditional)	MultiSTAAR-O (Conditional)	Variants (adjusted)
PCSK9	1	Putative loss-of-function	14	1.14E-115	2.66E-08	rs12117661, rs2495491, rs11591147, rs67608943, rs72646508, rs693668, rs28362261, rs28362263, rs141502002, rs505151, rs28362286
APOB	2	Putative loss-of-function	29	8.04E-28	5.76E-27	rs12478327, rs72654432, rs1042034, rs676210, rs533617, rs17240441, rs34722314, rs563290, rs10692845
ABCA1	9	Putative loss-of-function	28	2.04E-21	5.41E-21	rs2150867, rs33918808, rs112853430, rs4149307, rs9282541, rs1883025, rs1800978
LDLR	19	Putative loss-of-function	19	8.81E-21	7.16E-21	rs140753491, rs138294113, rs17242353, rs17242843, rs10422256, rs72658860, rs11669576, rs2738447, rs72658867, rs2738464, rs6511728, rs3760782, rs59168178, rs2278426, rs112942459
PCSK9	1	Missense	271	8.94E-71	1.29E-10	rs12117661, rs2495491, rs11591147, rs67608943, rs72646508, rs693668, rs28362261, rs28362263, rs141502002, rs505151, rs28362286
APOB	2	Missense	1407	5.57E-08	4.31E-08	rs12478327, rs72654432, rs1042034, rs676210, rs533617, rs17240441, rs34722314, rs563290, rs10692845
ABCG5	2	Missense	242	5.75E-08	9.81E-08	rs114780578, rs11887534, rs4245791
NPC1L1	7	Missense	477	3.10E-08	1.60E-07	rs217381
LPL	8	Missense	149	9.57E-19	7.14E-04	rs6996383, rs268, rs328, rs3289, rs13702, rs15285, rs78810414, rs28550053, rs12676079, rs55682243
ABCA1	9	Missense	597	3.63E-46	1.75E-33	rs2150867, rs33918808, rs112853430, rs4149307, rs9282541, rs1883025, rs1800978
SCARB1	12	Missense	192	6.77E-15	3.55E-15	rs6488913, rs4765127, rs1716407, rs825456, rs1672875, rs10846744, rs10773112, rs187471874, rs10773119
LIPC	15	Missense	246	2.54E-20	6.66E-15	rs1973688, rs1601935, rs2043082, rs10468017, rs1532085, rs436965, rs35980001, rs1800588, rs2070895, rs113298164
CETP	16	Missense	168	8.84E-14	2.09E-04	rs35571500, rs247617, rs17231506, rs34498052, rs34119551, rs34065661, rs1597000001*, rs7499892, rs5883, rs289719, rs11860407, rs189866004,

						rs5880
<i>LCAT</i>	16	Missense	107	9.18E-14	3.06E-17	rs111315946, rs150660813, rs4986970, rs35673026, rs1109166, rs548291389, rs140753491, rs138294113, rs17242353, rs17242843, rs10422256, rs72658860, rs11669576, rs2738447, rs72658867, rs2738464, rs6511728, rs3760782, rs59168178, rs2278426, rs112942459
<i>LDLR</i>	19	Missense	342	7.92E-58	2.12E-57	
<i>TM6SF2</i>	19	Missense	120	7.06E-08	6.16E-07	rs3761077, rs150641967, rs187429064, rs2074304
<i>PCSK9</i>	1	Putative loss-of-function and disruptive missense	71	1.14E-107	8.22E-17	rs12117661, rs2495491, rs11591147, rs67608943, rs72646508, rs693668, rs28362261, rs28362263, rs141502002, rs505151, rs28362286
<i>APOB</i>	2	Putative loss-of-function and disruptive missense	75	9.96E-12	9.86E-12	rs12478327, rs72654432, rs1042034, rs676210, rs533617, rs17240441, rs34722314, rs563290, rs10692845
<i>NPC1L1</i>	7	Putative loss-of-function and disruptive missense	303	1.79E-09	8.29E-09	rs217381
<i>ABCA1</i>	9	Putative loss-of-function and disruptive missense	357	7.85E-33	2.66E-33	rs2150867, rs33918808, rs112853430, rs4149307, rs9282541, rs1883025, rs1800978
<i>APOC3</i>	11	Putative loss-of-function and disruptive missense	15	2.86E-126	3.01E-06	rs509728, rs61905072, rs66505542, rs7102314, rs964184, rs75198898, rs142958146, rs2075291, rs3135506, rs651821, rs45611741, rs662799, rs10750097, rs9804646, rs978880643, rs2070669, rs76353203, rs138326449, rs147210663, rs140621530, rs525028, rs141469619, rs188287950, rs202207736
<i>SCARB1</i>	12	Putative loss-of-function and disruptive missense	60	3.49E-17	2.14E-17	rs6488913, rs4765127, rs1716407, rs825456, rs1672875, rs10846744, rs10773112, rs187471874, rs10773119
<i>LIPC</i>	15	Putative loss-of-function and disruptive missense	130	1.01E-19	1.49E-17	rs1973688, rs1601935, rs2043082, rs10468017, rs1532085, rs436965, rs35980001, rs1800588, rs2070895, rs113298164
<i>LCAT</i>	16	Putative loss-of-function and disruptive missense	88	2.38E-16	5.07E-17	rs111315946, rs150660813, rs4986970, rs35673026, rs1109166, rs548291389, rs140753491, rs138294113, rs17242353, rs17242843, rs10422256, rs72658860, rs11669576, rs2738447, rs72658867, rs2738464, rs6511728, rs3760782, rs59168178, rs2278426, rs112942459
<i>LDLR</i>	19	Putative loss-of-function and disruptive missense	221	6.97E-72	1.57E-71	
<i>PCSK9</i>	1	Disruptive missense	57	7.03E-19	1.33E-12	rs12117661, rs2495491, rs11591147, rs67608943, rs72646508, rs693668, rs28362261, rs28362263, rs141502002, rs505151, rs28362286
<i>APOB</i>	2	Disruptive missense	46	5.78E-09	4.48E-09	rs12478327, rs72654432, rs1042034, rs676210, rs533617, rs17240441, rs34722314, rs563290, rs10692845
<i>NPC1L1</i>	7	Disruptive missense	276	3.34E-09	1.57E-08	rs217381
<i>ABCA1</i>	9	Disruptive missense	329	1.17E-22	1.59E-23	rs2150867, rs33918808, rs112853430, rs4149307, rs9282541, rs1883025, rs1800978
<i>APOC3</i>	11	Disruptive missense	6	2.38E-29	3.93E-04	rs509728, rs61905072, rs66505542, rs7102314, rs964184, rs75198898, rs142958146, rs2075291, rs3135506,

						rs651821, rs45611741, rs662799, rs10750097, rs9804646, rs978880643, rs2070669, rs76353203, rs138326449, rs147210663, rs140621530, rs525028, rs141469619, rs188287950, rs202207736
SCARB1	12	Disruptive missense	51	4.44E-16	2.86E-16	rs6488913, rs4765127, rs1716407, rs825456, rs1672875, rs10846744, rs10773112, rs187471874, rs10773119 rs1973688, rs1601935, rs2043082, rs10468017,
LIPC	15	Disruptive missense	112	2.19E-18	2.65E-16	rs1532085, rs436965, rs35980001, rs1800588, rs2070895, rs113298164
LCAT	16	Disruptive missense	84	2.85E-14	6.44E-15	rs111315946, rs150660813, rs4986970, rs35673026, rs1109166, rs548291389 rs140753491, rs138294113, rs17242353, rs17242843, rs10422256,
LDLR	19	Disruptive missense	203	2.22E-59	5.13E-59	rs72658860, rs11669576, rs2738447, rs72658867, rs2738464, rs6511728, rs3760782, rs59168178, rs2278426, rs112942459

698 * Samoan-specific missense variant.

699

700

701

702

703

704

705 **Table 2 | TOPMed Gene-centric noncoding multi-trait analysis results of both**
 706 **unconditional analysis and analysis conditional on known lipids-associated**
 707 **variants.** A total of 61,838 samples from the TOPMed Program were considered in the
 708 analysis. Results for the conditionally significant genes (unconditional MultiSTAAR-O
 709 $P < 3.57 \times 10^{-7}$ and conditional MultiSTAAR-O $P < 6.58 \times 10^{-4}$ for 7 different
 710 noncoding masks across protein-coding genes; unconditional MultiSTAAR-O $P <$
 711 2.50×10^{-6} and conditional MultiSTAAR-O $P < 8.33 \times 10^{-3}$ for ncRNA genes) are
 712 presented in the table. MultiSTAAR-O is a two-sided test. Chr. no., chromosome
 713 number; Category, functional category; No. of SNVs, number of rare variants (MAF <
 714 1%) of the particular noncoding functional category in the gene; MultiSTAAR-O,
 715 MultiSTAAR-O P value; Variants (adjusted), adjusted variants in the conditional
 716 analysis; n/a, no variant adjusted in the conditional analysis.

717

Gene	Chr. no.	Category	No. of SNVs	MultiSTAAR-O (Unconditional)	MultiSTAAR-O (Conditional)	Variants (adjusted)
<i>APOA1</i>	11	Promoter (CAGE)	230	2.33E-07	9.45E-07	rs509728, rs61905072, rs66505542, rs7102314, rs964184, rs75198898, rs142958146, rs2075291, rs3135506, rs651821, rs45611741, rs662799, rs10750097, rs9804646, rs978880643, rs2070669, rs76353203, rs138326449, rs147210663, rs140621530, rs525028, rs141469619, rs188287950, rs202207736
<i>CETP</i>	16	Promoter (DHS)	411	1.21E-12	5.75E-04	rs35571500, rs247617, rs17231506, rs34498052, rs34119551, rs34065661, rs1597000001*, rs7499892, rs5883, rs289719, rs11860407, rs189866004, rs5880
<i>APOA1</i>	11	Enhancer (CAGE)	642	1.88E-24	6.23E-04	rs509728, rs61905072, rs66505542, rs7102314, rs964184, rs75198898, rs142958146, rs2075291, rs3135506, rs651821, rs45611741, rs662799, rs10750097, rs9804646, rs978880643, rs2070669, rs76353203, rs138326449, rs147210663, rs140621530, rs525028, rs141469619, rs188287950, rs202207736
<i>SPC24</i>	19	Enhancer (CAGE)	366	1.33E-08	4.88E-04	rs140753491, rs138294113, rs17242353, rs17242843, rs10422256, rs72658860, rs11669576, rs2738447, rs72658867, rs2738464, rs6511728, rs3760782, rs59168178, rs2278426, rs112942459
<i>NIPSNAP3A</i>	9	Enhancer (DHS)	767	2.63E-08	8.46E-06	rs2150867, rs33918808, rs112853430, rs4149307, rs9282541, rs1883025, rs1800978
<i>LIPC</i>	15	Enhancer (DHS)	3714	4.26E-08	1.25E-04	rs1973688, rs1601935, rs2043082, rs10468017, rs1532085, rs436965, rs35980001, rs1800588, rs2070895, rs113298164
<i>RP11-310H4.2</i>	7	ncRNA	154	1.69E-06	1.69E-06	n/a

<i>MIR4497</i>	12	ncRNA	23	1.37E-06	1.42E-06	rs5800864
<i>RP11-15F12.3</i>	18	ncRNA	64	7.53E-11	7.50E-03	rs77960347, rs117623631, rs9958734, rs7229562, rs8086351, rs10048323, rs8084172

718 * Samoan-specific missense variant.

719

720

721

722

723

724

725

726

727

728

729 **Table 3 | TOPMed Genetic region (2-kb sliding window) multi-trait analysis results**
730 **of both unconditional analysis and analysis conditional on known lipid-**
731 **associated variants.** A total of 61,838 samples from the TOPMed Program were
732 considered in the analysis. Results for the conditionally significant sliding windows
733 (unconditional MultiSTAAR-O $P < 1.89 \times 10^{-8}$ and conditional MultiSTAAR-O $P <$
734 9.96×10^{-5}) are presented in the table. MultiSTAAR-O is a two-sided test. Chr. no.,
735 chromosome number; Start location, start location of the 2-kb sliding window; End
736 location, end location of the 2-kb sliding window; No. of SNVs, number of rare variants
737 (MAF < 1%) in the 2-kb sliding window; MultiSTAAR-O, MultiSTAAR-O P value;
738 Variants (adjusted), adjusted variants in the conditional analysis; n/a, no variant
739 adjusted in the conditional analysis. Physical positions of each window are on build
740 hg38.

Chr. no.	Start location	End location	Gene	No. of SNVs	MultiSTAAR-O (Unconditional)	MultiSTAAR-O (Conditional)	Variants (adjusted)
1	55,051,447	55,053,446	PCSK9	327	7.11E-11	6.60E-08	rs12117661, rs2495491, rs11591147, rs67608943, rs72646508, rs693668, rs28362261, rs28362263, rs141502002, rs505151, rs28362286
1	55,052,447	55,054,446	PCSK9	320	9.37E-09	9.07E-06	rs12117661, rs2495491, rs11591147, rs67608943, rs72646508, rs693668, rs28362261, rs28362263, rs141502002, rs505151, rs28362286
1	62,651,447	62,653,446	DOCK7	277	5.08E-09	7.56E-10	rs67461605
1	62,652,447	62,654,446	DOCK7	257	4.87E-09	7.24E-10	rs67461605
1	145,530,447	145,532,446	intergenic	233	5.12E-09	5.12E-09	n/a
							rs140753491, rs138294113, rs17242353, rs17242843, rs10422256, rs72658860, rs11669576, rs2738447, rs72658867, rs2738464, rs6511728, rs3760782, rs59168178, rs2278426, rs112942459
19	11,104,367	11,106,366	LDLR	336	1.15E-12	8.33E-13	rs140753491, rs138294113, rs17242353, rs17242843, rs10422256, rs72658860, rs11669576, rs2738447, rs72658867, rs2738464, rs6511728, rs3760782, rs59168178, rs2278426, rs112942459
19	11,105,367	11,107,366	LDLR	338	5.97E-14	5.55E-15	rs140753491, rs138294113, rs17242353, rs17242843, rs10422256, rs72658860, rs11669576, rs2738447, rs72658867, rs2738464, rs6511728, rs3760782, rs59168178, rs2278426, rs112942459

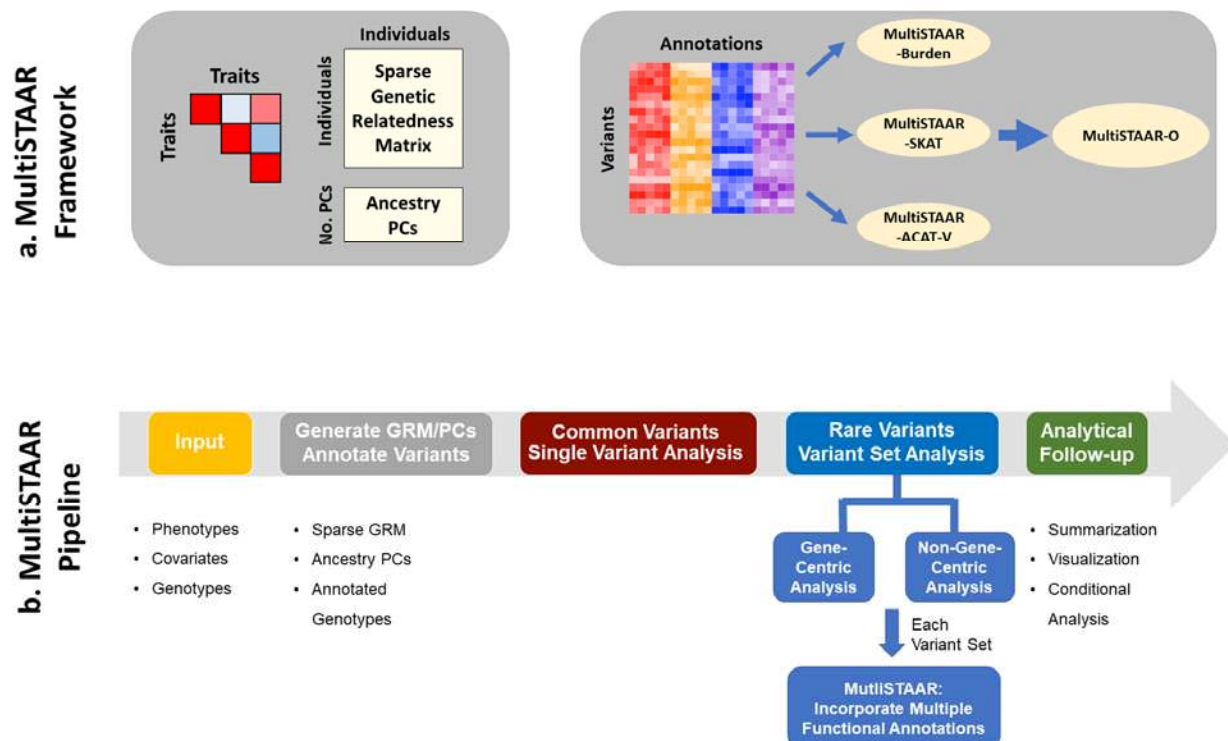
741 * Samoan-specific missense variant.

742

743

744 **FIGURES**

745 **Fig. 1 | MultiSTAAR framework and pipeline.** **a**, MultiSTAAR framework. (i) Fit null
746 Multivariate Linear Mixed Models (MLLMMs) using sparse GRM and ancestry PCs to
747 account for population structure, relatedness and the correlation between phenotypes.
748 (ii) Test for associations between each variant set and multiple traits by dynamically
749 incorporating multiple variant functional annotations. **b**, MultiSTAAR pipeline. (i) Prepare
750 the input data of MultiSTAAR, including genotypes, multiple phenotypes and covariates.
751 (ii) Calculate sparse GRM, ancestry PCs and annotate all variants in the genome. (iii)
752 Perform single variant analysis for common variants. (iv) Define the rare variant analysis
753 units, including gene-centric analysis of five coding functional categories and eight
754 noncoding functional categories and non-gene-centric analysis of sliding windows. (v)
755 Provide result summarization and perform analytical follow-up via conditional analysis.
756

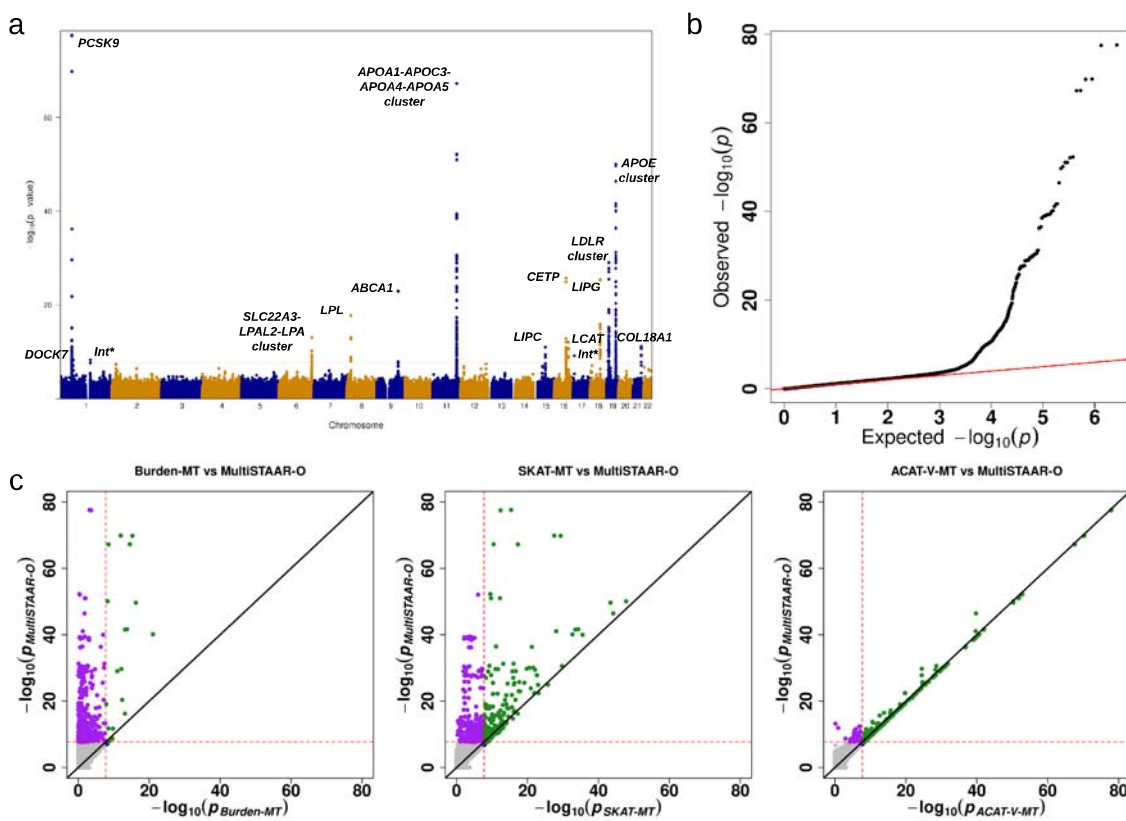


757

758

759

760 **Fig. 2 | TOPMed Genetic region (2-kb sliding window) unconditional multi-trait**
761 **analysis results of low-density lipoprotein cholesterol (LDL-C), high-density**
762 **lipoprotein cholesterol (HDL-C) and triglycerides (TG) using TOPMed data. a,**
763 **Manhattan plot showing the associations of 2.65 million 2-kb sliding windows versus**
764 **$-\log_{10}(P)$ of MultiSTAAR-O. The horizontal line indicates a genome-wide P value**
765 **threshold of 1.89×10^{-8} ($n = 61,838$). b, Quantile-quantile plot of 2-kb sliding window**
766 **MultiSTAAR-O P values ($n = 61,838$). c, Scatterplot of P values for the 2-kb sliding**
767 **windows comparing MultiSTAAR-O with Burden-MT, SKAT-MT and ACAT-V-MT tests**
768 **(MT is short for Multi-Trait). Each dot represents a sliding window with x-axis label being**
769 **$-\log_{10}(P)$ of the conventional multi-trait test and y-axis label being the $-\log_{10}(P)$ of**
770 **MultiSTAAR-O ($n = 61,838$). Burden-MT, SKAT-MT, ACAT-V-MT and MultiSTAAR-O**
771 **are two-sided tests. Int*, intergenic sliding window.**



772

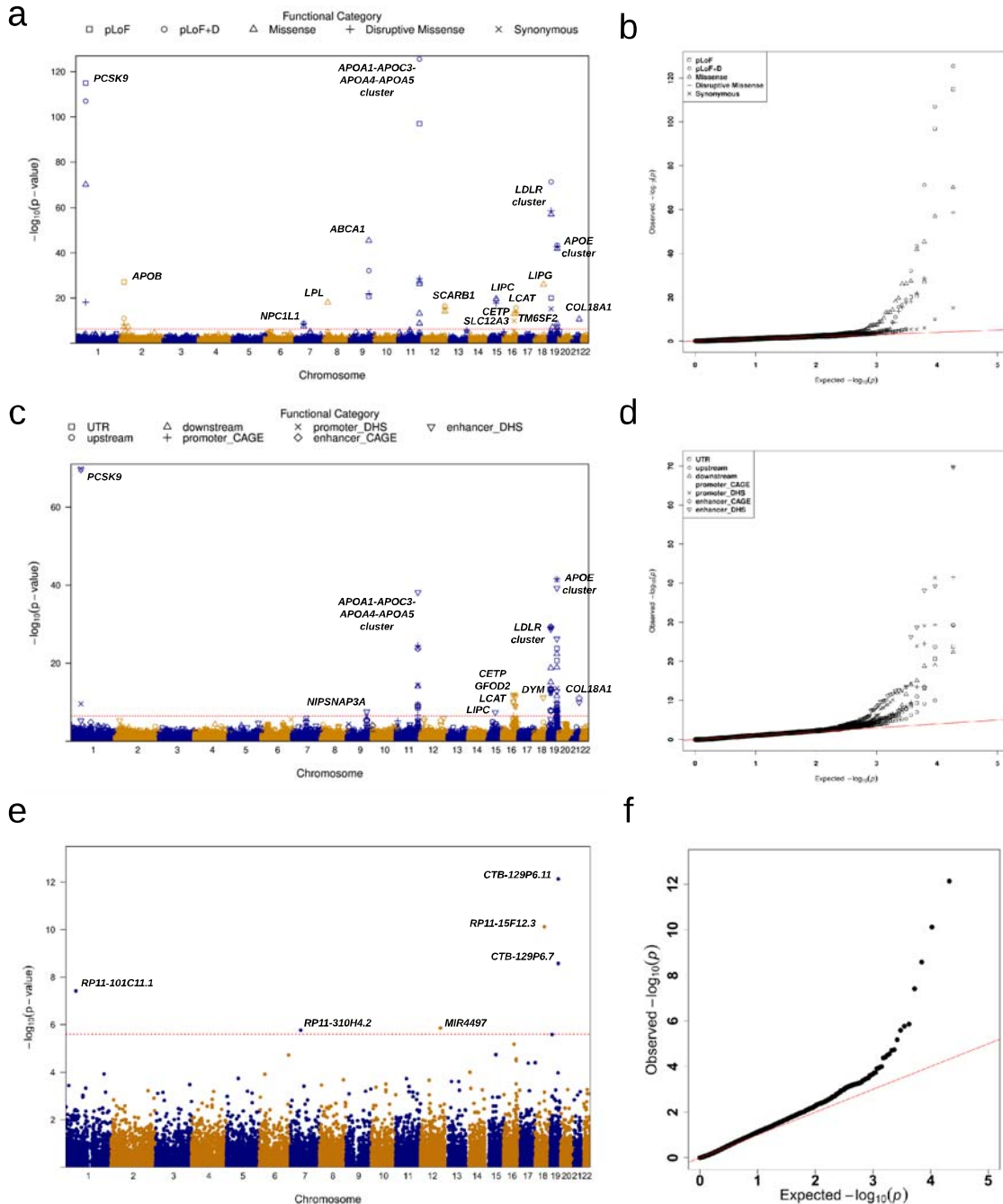
773

774

775 **EXTENDED DATA FIGURES**

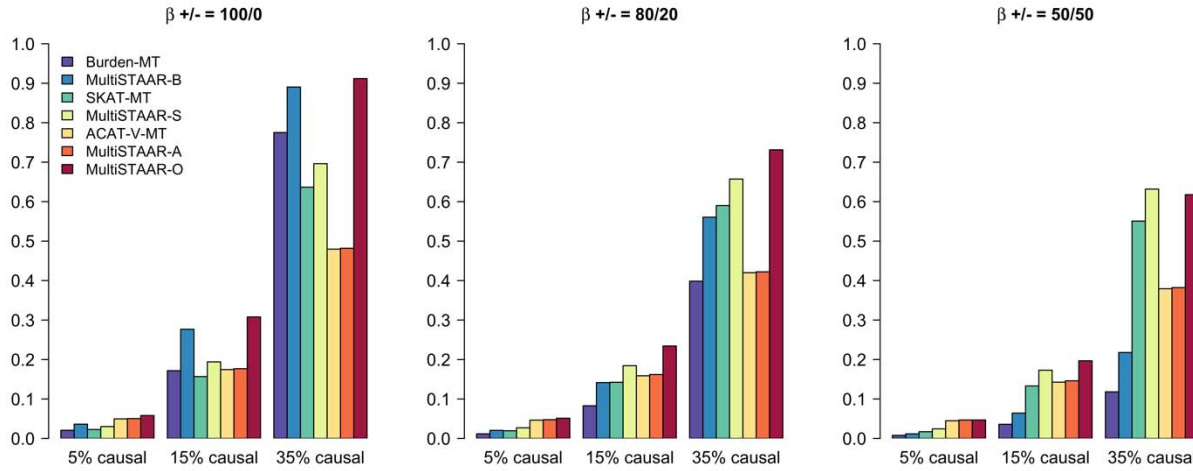
776 **Extended Data Fig. 1 | Manhattan plots and Q-Q plots for unconditional**
777 **gene-centric coding, noncoding and ncRNA analysis of low-density lipoprotein**
778 **cholesterol (LDL-C), high-density lipoprotein cholesterol (HDL-C) and triglycerids**
779 **(TG) using TOPMed data (n = 61,838).** **a**, Manhattan plots for unconditional gene-
780 centric coding analysis of protein-coding gene. The horizontal line indicates a genome-
781 wide MultiSTAAR-O *P* value threshold of 5.00×10^{-7} . The significant threshold is
782 defined by multiple comparisons using the Bonferroni correction ($0.05 / (20,000 \times 5) =$
783 5.00×10^{-7}). Different symbols represent the MultiSTAAR-O *P* value of the protein-
784 coding gene using different functional categories (putative loss-of-function, putative
785 loss-of-function and disruptive missense, missense, disruptive missense, synonymous).
786 **b**, Quantile-quantile plots for unconditional gene-centric coding analysis of protein-
787 coding gene. Different symbols represent the MultiSTAAR-O *P*-value of the gene using
788 different functional categories. **c**, Manhattan plots for unconditional gene-centric
789 noncoding analysis of protein-coding gene. The horizontal line indicates a genome-wide
790 MultiSTAAR-O *P* value threshold of 3.57×10^{-7} . The significant threshold is defined by
791 multiple comparisons using the Bonferroni correction ($0.05 / (20,000 \times 7) = 3.57 \times 10^{-7}$).
792 Different symbols represent the MultiSTAAR-O *P* value of the protein-coding gene using
793 different functional categories (upstream, downstream, UTR, promoter_CAGE,
794 promoter_DHS, enhancer_CAGE, enhancer_DHS). Promoter_CAGE and
795 promoter_DHS are the promoters with overlap of Cap Analysis of Gene Expression
796 (CAGE) sites and DNase hypersensitivity (DHS) sites for a given gene, respectively.
797 Enhancer_CAGE and enhancer_DHS are the enhancers in GeneHancer predicted
798 regions with the overlap of CAGE sites and DHS sites for a given gene, respectively. **d**,
799 Quantile-quantile plots for unconditional gene-centric noncoding analysis of protein-
800 coding gene. Different symbols represent the MultiSTAAR-O *P*-value of the gene using
801 different functional categories. **e**, Manhattan plots for unconditional gene-centric
802 noncoding analysis of ncRNA gene. The horizontal line indicates a genome-wide
803 MultiSTAAR-O *P* value threshold of 2.50×10^{-6} . The significant threshold is defined by
804 multiple comparisons using the Bonferroni correction ($0.05 / 20,000 = 2.50 \times 10^{-6}$). **f**,
805 Quantile-quantile plots for unconditional gene-centric noncoding analysis of ncRNA

806 gene. In panels, **a**, **c** and **e**, the chromosome number are indicated by the colors of
 807 dots. In all panels, MultiSTAAR-O is a two-sided test.

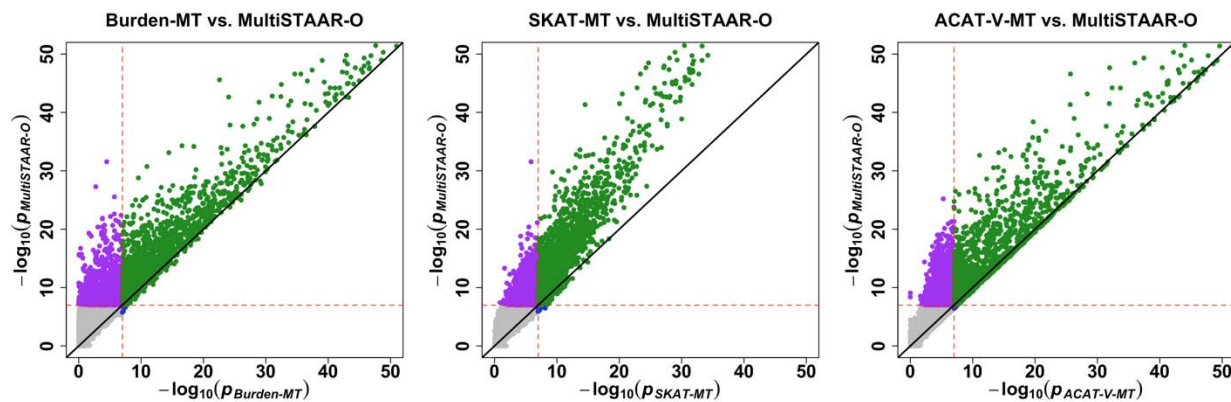


808
 809
 810

811 **Extended Data Fig. 2 | Power comparisons of Burden-MT, SKAT-MT, ACAT-V-MT**
812 **(MT is short for Multi-Trait) and MultiSTAAR methods when variants in the signal**
813 **region are associated with one phenotype.** Multi-trait Burden, SKAT and ACAT-V-
814 tests implemented in MultiSTAAR are denoted by Burden-MT, SKAT-MT and ACAT-V-
815 MT. MultiSTAAR methods incorporating ten functional annotations are denoted by
816 MultiSTAAR-B, MultiSTAAR-S, MultiSTAAR-A and MultiSTAAR-O. In each simulation
817 replicate, a 5-kb region was randomly selected as the signal region. Within each signal
818 region, variants were randomly generated to be causal based on the multivariate logistic
819 model and on average there were 5%, 15% or 35% causal variants in the signal region.
820 The effect sizes of causal variants were $\beta_j = c_0 |\log_{10} MAF_j|$, where c_0 was set to be
821 0.13. The barplot of power in the top panel consider settings in which the effect sizes for
822 the causal variants are 100% positive (0% negative), 80% positive (20% negative), and
823 50% positive (50% negative). The scatterplot of P values in the bottom panel compare
824 MultiSTAAR-O to Burden-MT, SKAT-MT and ACAT-V-MT when 15% of variants in the
825 signal region are causal variants with all positive effect sizes. Power was estimated as
826 the proportion of the P values less than $\alpha = 10^{-7}$ based on 10^4 replicates. Burden-MT,
827 SKAT-MT, ACAT-V-MT, MultiSTAAR-B, MultiSTAAR-S, MultiSTAAR-A and
828 MultiSTAAR-O are two-sided tests. Total sample size considered was 10,000.



829



830

831

832

833

834

835

836

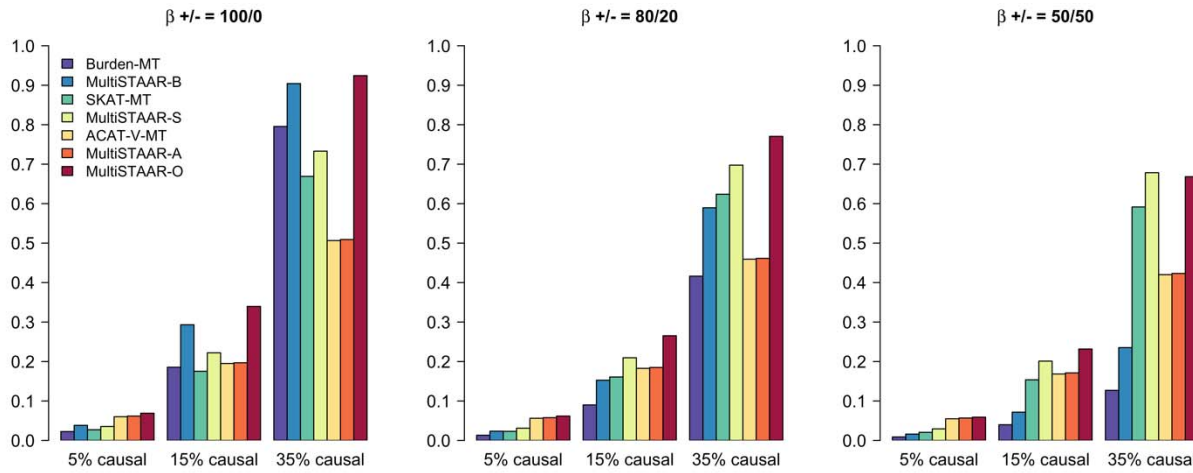
837

838

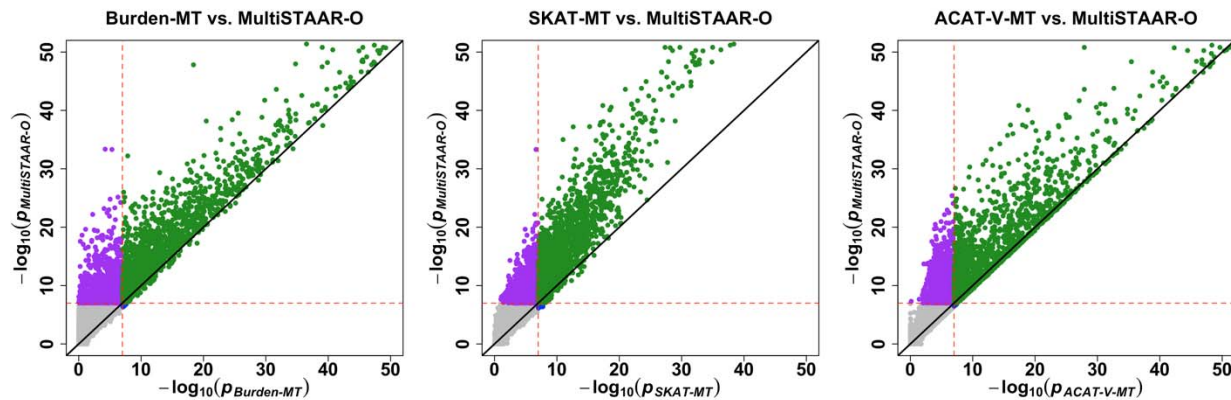
839

840

841 **Extended Data Fig. 3 | Power comparisons of Burden-MT, SKAT-MT, ACAT-V-MT**
842 **(MT is short for Multi-Trait) and MultiSTAAR methods when variants in the signal**
843 **region are associated with two positively correlated phenotypes.** In each
844 simulation replicate, a 5-kb region was randomly selected as the signal region. Within
845 each signal region, variants were randomly generated to be causal based on the
846 multivariate logistic model and on average there were 5%, 15% or 35% causal variants
847 in the signal region. The effect sizes of causal variants were $\beta_j = c_0 |\log_{10} MAF_j|$, where
848 c_0 was set to be 0.1. The barplot of power in the top panel consider settings in which the
849 effect sizes for the causal variants are 100% positive (0% negative), 80% positive (20%
850 negative), and 50% positive (50% negative). The scatterplot of P values in the bottom
851 panel compare MultiSTAAR-O to Burden-MT, SKAT-MT and ACAT-V-MT when 15% of
852 variants in the signal region are causal variants with all positive effect sizes. Power was
853 estimated as the proportion of the P values less than $\alpha = 10^{-7}$ based on 10^4 replicates.
854 Burden-MT, SKAT-MT, ACAT-V-MT, MultiSTAAR-B, MultiSTAAR-S, MultiSTAAR-A and
855 MultiSTAAR-O are two-sided tests. Total sample size considered was 10,000.
856
857



858



859

860

861

862

863

864

865

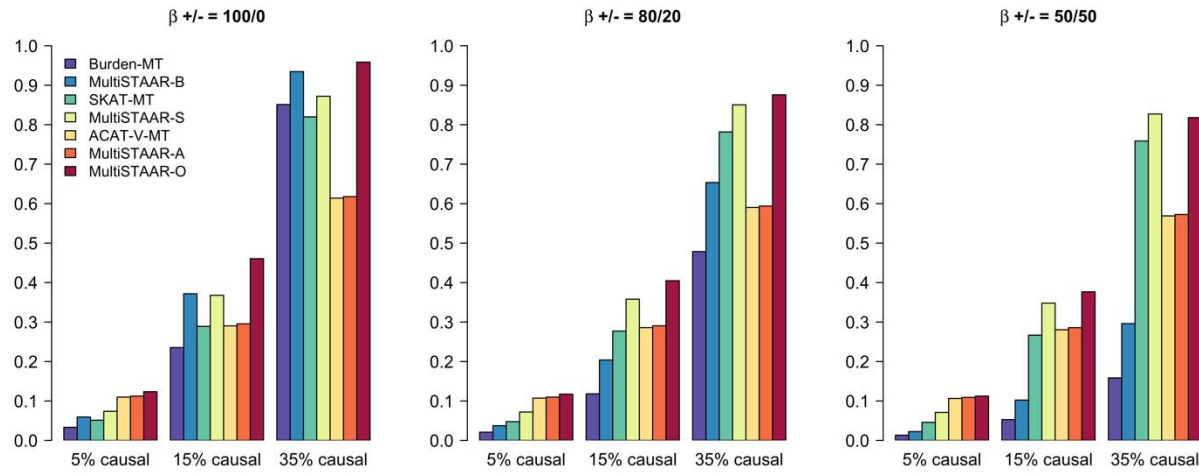
866

867

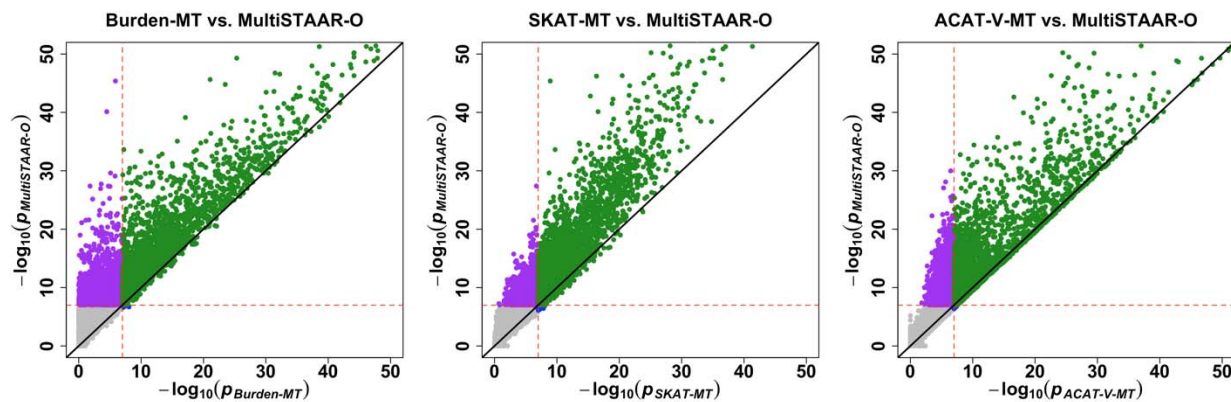
868

869

870 **Extended Data Fig. 4 | Power comparisons of Burden-MT, SKAT-MT, ACAT-V-MT**
871 **(MT is short for Multi-Trait) and MultiSTAAR methods when variants in the signal**
872 **region are associated with two negatively correlated phenotypes.** In each
873 simulation replicate, a 5-kb region was randomly selected as the signal region. Within
874 each signal region, variants were randomly generated to be causal based on the
875 multivariate logistic model and on average there were 5%, 15% or 35% causal variants
876 in the signal region. The effect sizes of causal variants were $\beta_j = c_0 |\log_{10} MAF_j|$, where
877 c_0 was set to be 0.1. The barplot of power in the top panel consider settings in which the
878 effect sizes for the causal variants are 100% positive (0% negative), 80% positive (20%
879 negative), and 50% positive (50% negative). The scatterplot of P values in the bottom
880 panel compare MultiSTAAR-O to Burden-MT, SKAT-MT and ACAT-V-MT when 15% of
881 variants in the signal region are causal variants with all positive effect sizes. Power was
882 estimated as the proportion of the P values less than $\alpha = 10^{-7}$ based on 10^4 replicates.
883 Burden-MT, SKAT-MT, ACAT-V-MT, MultiSTAAR-B, MultiSTAAR-S, MultiSTAAR-A and
884 MultiSTAAR-O are two-sided tests. Total sample size considered was 10,000.
885
886



887



888

889

890

891

892

893

894

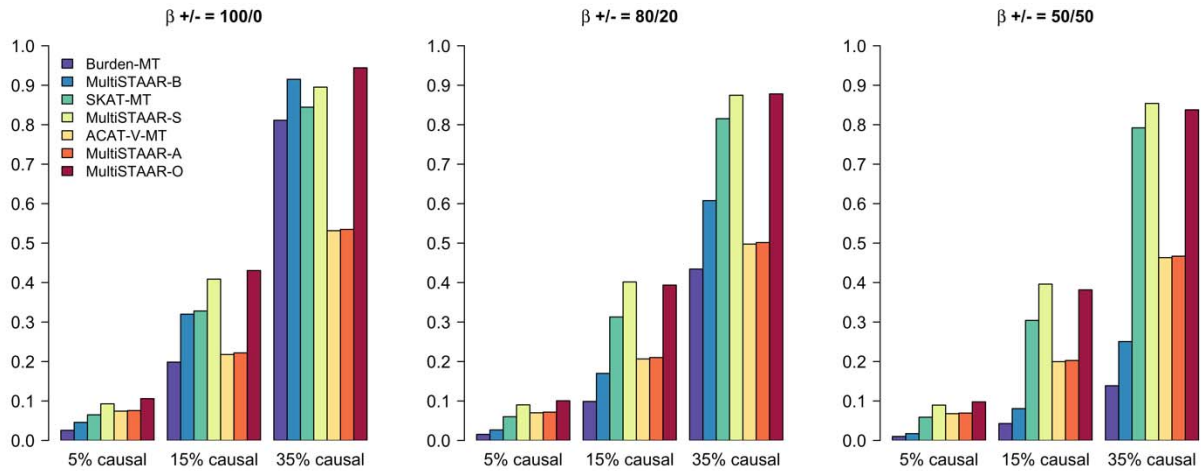
895

896

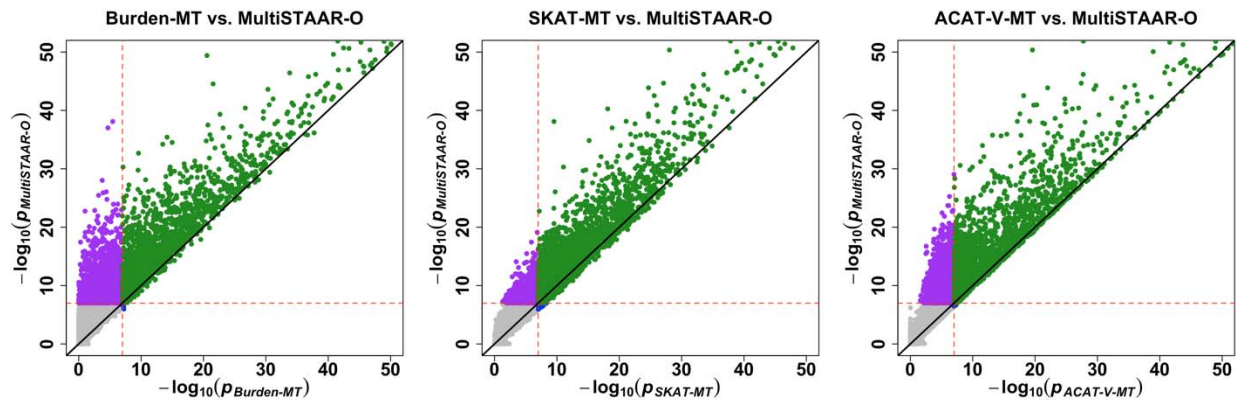
897

898

899 **Extended Data Fig. 5 | Power comparisons of Burden-MT, SKAT-MT, ACAT-V-MT**
900 **(MT is short for Multi-Trait) and MultiSTAAR methods when variants in the signal**
901 **region are associated with three phenotypes.** In each simulation replicate, a 5-kb
902 region was randomly selected as the signal region. Within each signal region, variants
903 were randomly generated to be causal based on the multivariate logistic model and on
904 average there were 5%, 15% or 35% causal variants in the signal region. The effect
905 sizes of causal variants were $\beta_j = c_0 |\log_{10} MAF_j|$, where c_0 was set to be 0.07. The
906 barplot of power in the top panel consider settings in which the effect sizes for the
907 causal variants are 100% positive (0% negative), 80% positive (20% negative), and
908 50% positive (50% negative). The scatterplot of P values in the bottom panel compare
909 MultiSTAAR-O to Burden-MT, SKAT-MT and ACAT-V-MT when 15% of variants in the
910 signal region are causal variants with all positive effect sizes. Power was estimated as
911 the proportion of the P values less than $\alpha = 10^{-7}$ based on 10^4 replicates. Burden-MT,
912 SKAT-MT, ACAT-V-MT, MultiSTAAR-B, MultiSTAAR-S, MultiSTAAR-A and
913 MultiSTAAR-O are two-sided tests. Total sample size considered was 10,000.
914
915



916



917

918

919

920

921

922

923

924

925

926

927

928 **References**

- 929 1. Taliun, D. *et al.* Sequencing of 53,831 diverse genomes from the NHLBI
930 TOPMed Program. *Nature* **590**, 290-299 (2021).
- 931 2. The “All of Us” Research Program. *New England Journal of Medicine* **381**, 668-
932 676 (2019).
- 933 3. Halldorsson, B.V. *et al.* The sequences of 150,119 genomes in the UK Biobank.
934 *Nature* **607**, 732-740 (2022).
- 935 4. Lee, S., Abecasis, Gonçalo R., Boehnke, M. & Lin, X. Rare-Variant Association
936 Analysis: Study Designs and Statistical Tests. *The American Journal of Human
937 Genetics* **95**, 5-23 (2014).
- 938 5. Li, B. & Leal, S.M. Methods for Detecting Associations with Rare Variants for
939 Common Diseases: Application to Analysis of Sequence Data. *The American
940 Journal of Human Genetics* **83**, 311-321 (2008).
- 941 6. Madsen, B.E. & Browning, S.R. A Groupwise Association Test for Rare
942 Mutations Using a Weighted Sum Statistic. *PLOS Genetics* **5**, e1000384 (2009).
- 943 7. Morris, A.P. & Zeggini, E. An evaluation of statistical approaches to rare variant
944 analysis in genetic association studies. *Genetic Epidemiology* **34**, 188-193
(2010).
- 945 8. Wu, Michael C. *et al.* Rare-Variant Association Testing for Sequencing Data with
946 the Sequence Kernel Association Test. *The American Journal of Human
947 Genetics* **89**, 82-93 (2011).
- 948 9. Liu, Y. *et al.* ACAT: A Fast and Powerful p Value Combination Method for Rare-
949 Variant Analysis in Sequencing Studies. *The American Journal of Human
950 Genetics* **104**, 410-421 (2019).
- 951 10. Solovieff, N., Cotsapas, C., Lee, P.H., Purcell, S.M. & Smoller, J.W. Pleiotropy in
952 complex traits: challenges and strategies. *Nature Reviews Genetics* **14**, 483-495
(2013).
- 953 11. Sivakumaran, S. *et al.* Abundant Pleiotropy in Human Complex Diseases and
954 Traits. *The American Journal of Human Genetics* **89**, 607-618 (2011).
- 955 12. Abdellaoui, A., Yengo, L., Verweij, K.J.H. & Visscher, P.M. 15 years of GWAS
956 discovery: Realizing the promise. *The American Journal of Human Genetics*
(2023).
- 957 13. Watanabe, K. *et al.* A global overview of pleiotropy and genetic architecture in
958 complex traits. *Nature Genetics* **51**, 1339-1348 (2019).
- 959 14. Wu, B. & Pankow, J.S. Sequence Kernel Association Test of Multiple Continuous
960 Phenotypes. *Genetic Epidemiology* **40**, 91-100 (2016).
- 961 15. Dutta, D., Scott, L., Boehnke, M. & Lee, S. Multi-SKAT: General framework to
962 test for rare-variant association with multiple phenotypes. *Genetic Epidemiology*
963 **43**, 4-23 (2019).
- 964 16. Luo, L. *et al.* Multi-trait analysis of rare-variant association summary statistics
965 using MTAR. *Nature Communications* **11**, 2850 (2020).
- 966 17. Broadway, K.A. *et al.* A Statistical Approach for Testing Cross-Phenotype
967 Effects of Rare Variants. *The American Journal of Human Genetics* **98**, 525-540
(2016).

- 972 18. Li, X. *et al.* Dynamic incorporation of multiple in silico functional annotations
973 empowers rare variant association analysis of large whole-genome sequencing
974 studies at scale. *Nature Genetics* **52**, 969-983 (2020).
- 975 19. Sammel, M., Lin, X. & Ryan, L. Multivariate linear mixed models for multiple
976 outcomes. *Statistics in Medicine* **18**, 2479-2492 (1999).
- 977 20. Conomos, M.P., Miller, M.B. & Thornton, T.A. Robust Inference of Population
978 Structure for Ancestry Prediction and Correction of Stratification in the Presence
979 of Relatedness. *Genetic Epidemiology* **39**, 276-293 (2015).
- 980 21. Conomos, Matthew P., Reiner, Alexander P., Weir, Bruce S. & Thornton,
981 Timothy A. Model-free Estimation of Recent Genetic Relatedness. *The American
982 Journal of Human Genetics* **98**, 127-148 (2016).
- 983 22. Gogarten, S.M. *et al.* Genetic association testing using the GENESIS
984 R/Bioconductor package. *Bioinformatics* **35**, 5346-5348 (2019).
- 985 23. Lee, P.H. *et al.* Principles and methods of in-silico prioritization of non-coding
986 regulatory variants. *Human Genetics* **137**, 15-30 (2018).
- 987 24. Li, Z. *et al.* A framework for detecting noncoding rare-variant associations of
988 large-scale whole-genome sequencing studies. *Nature Methods* **19**, 1599-1611
989 (2022).
- 990 25. Morrison, A.C. *et al.* Practical approaches for whole-genome sequence analysis
991 of heart-and blood-related traits. *The American Journal of Human Genetics* **100**,
992 205-215 (2017).
- 993 26. Selvaraj, M.S. *et al.* Whole genome sequence analysis of blood lipid levels in
994 >66,000 individuals. *Nature Communications* **13**, 5995 (2022).
- 995 27. Liu, Z. & Lin, X. Multiple phenotype association tests using summary statistics in
996 genome-wide association studies. *Biometrics* **74**, 165-175 (2018).
- 997 28. Teslovich, T.M. *et al.* Biological, clinical and population relevance of 95 loci for
998 blood lipids. *Nature* **466**, 707 (2010).
- 999 29. Schaffner, S.F. *et al.* Calibrating a coalescent simulation of human genome
1000 sequence variation. *Genome research* **15**, 1576-1583 (2005).
- 1001 30. Natarajan, P. *et al.* Deep-coverage whole genome sequences and blood lipids
1002 among 16,324 individuals. *Nature Communications* **9**, 3391 (2018).
- 1003 31. Stilp, A.M. *et al.* A System for Phenotype Harmonization in the National Heart,
1004 Lung, and Blood Institute Trans-Omics for Precision Medicine (TOPMed)
1005 Program. *American Journal of Epidemiology* (2021).
- 1006 32. Frankish, A. *et al.* GENCODE reference annotation for the human and mouse
1007 genomes. *Nucleic acids research* **47**, D766-D773 (2019).
- 1008 33. Dong, C. *et al.* Comparison and integration of deleteriousness prediction
1009 methods for nonsynonymous SNVs in whole exome sequencing studies. *Human
1010 Molecular Genetics* **24**, 2125-2137 (2014).
- 1011 34. Li, Z. *et al.* A framework for detecting noncoding rare variant associations of
1012 large-scale whole-genome sequencing studies. *bioRxiv*, 2021.11.05.467531
1013 (2021).
- 1014 35. Kircher, M. *et al.* A general framework for estimating the relative pathogenicity of
1015 human genetic variants. *Nature Genetics* **46**, 310-315 (2014).

- 1016 36. Huang, Y.-F., Gulko, B. & Siepel, A. Fast, scalable prediction of deleterious
1017 noncoding variants from functional and population genomic data. *Nature Genetics* **49**, 618-624 (2017).
- 1018 37. Rogers, M.F. *et al.* FATHMM-XF: accurate prediction of pathogenic point
1019 mutations via extended features. *Bioinformatics* **34**, 511-513 (2017).
- 1020 38. Buniello, A. *et al.* The NHGRI-EBI GWAS Catalog of published genome-wide
1021 association studies, targeted arrays and summary statistics 2019. *Nucleic Acids
1022 Research* **47**, D1005-D1012 (2019).
- 1023 39. Klarin, D. *et al.* Genetics of blood lipids among ~300,000 multi-ethnic participants
1024 of the Million Veteran Program. *Nature Genetics* **50**, 1514-1523 (2018).
- 1025 40. Forrest, A.R. *et al.* A promoter-level mammalian expression atlas. *Nature* **507**,
1026 462 (2014).
- 1027 41. Abascal, F. *et al.* Expanded encyclopaedias of DNA elements in the human and
1028 mouse genomes. *Nature* **583**, 699-710 (2020).
- 1029 42. Andersson, R. *et al.* An atlas of active enhancers across human cell types and
1030 tissues. *Nature* **507**, 455-461 (2014).
- 1031 43. Fishilevich, S. *et al.* GeneHancer: genome-wide integration of enhancers and
1032 target genes in GeneCards. *Database* **2017**(2017).
- 1033 44. Li, Z. *et al.* Dynamic Scan Procedure for Detecting Rare-Variant Association
1034 Regions in Whole-Genome Sequencing Studies. *The American Journal of
1035 Human Genetics* **104**, 802-814 (2019).
- 1036 45. McCaw, Z.R., Gao, J., Lin, X. & Gronsbell, J. Leveraging a machine learning
1037 derived surrogate phenotype to improve power for genome-wide association
1038 studies of partially missing phenotypes in population biobanks. *bioRxiv*,
1039 2022.12.12.520180 (2022).
- 1040 46. Li, X. *et al.* Powerful, scalable and resource-efficient meta-analysis of rare variant
1041 associations in large whole genome sequencing studies. *Nature Genetics* **55**,
1042 154-164 (2023).
- 1043 47. Chen, H. *et al.* Control for Population Structure and Relatedness for Binary Traits
1044 in Genetic Association Studies via Logistic Mixed Models. *The American Journal
1045 of Human Genetics* **98**, 653-666 (2016).
- 1046 48. Chen, H. *et al.* Efficient Variant Set Mixed Model Association Tests for
1047 Continuous and Binary Traits in Large-Scale Whole-Genome Sequencing
1048 Studies. *The American Journal of Human Genetics* **104**, 260-274 (2019).
- 1049 49. Liu, Y. & Xie, J. Cauchy combination test: a powerful test with analytic p-value
1050 calculation under arbitrary dependency structures. *Journal of the American
1051 Statistical Association* **115**, 393-402 (2020).
- 1052
1053
1054
- 1055
1056
1057

1058 **Methods**

1059 **Ethics statement**

1060 This study relied on analyses of genetic data from TOPMed cohorts. The study has
1061 been approved by the TOPMed Publications Committee, TOPMed Lipids Working
1062 Group and all the participating cohorts, including Old Order Amish (phs000956.v1.p1),
1063 Atherosclerosis Risk in Communities Study (phs001211), Mt Sinai BioMe Biobank
1064 (phs001644), Coronary Artery Risk Development in Young Adults (phs001612),
1065 Cleveland Family Study (phs000954), Cardiovascular Health Study (phs001368),
1066 Diabetes Heart Study (phs001412), Framingham Heart Study (phs000974), Genetic
1067 Study of Atherosclerosis Risk (phs001218), Genetic Epidemiology Network of
1068 Arteriopathy (phs001345), Genetic Epidemiology Network of Salt Sensitivity
1069 (phs001217), Genetics of Lipid Lowering Drugs and Diet Network (phs001359),
1070 Hispanic Community Health Study - Study of Latinos (phs001395), Hypertension
1071 Genetic Epidemiology Network and Genetic Epidemiology Network
1072 of Arteriopathy (phs001293), Jackson Heart Study (phs000964), Multi-Ethnic Study of
1073 Atherosclerosis (phs001416), San Antonio Family Heart Study (phs001215), Genome-
1074 wide Association Study of Adiposity in Samoans (phs000972), Taiwan Study of
1075 Hypertension using Rare Variants (phs001387), and Women's Health Initiative
1076 (phs001237), where the accession numbers are provided in parenthesis. The use of
1077 human genetics data from TOPMed cohorts was approved by the Harvard T.H. Chan
1078 School of Public Health IRB (IRB13-0353).

1079

1080 **Notation and model**

1081 Suppose there are n subjects with a total of M variants sequenced across the whole
 1082 genome. For the i -th subject, let $\mathbf{Y}_i = (y_{i1}, y_{i2}, \dots, y_{iK})^T$ denote a vector of K quantitative
 1083 phenotypes; $\mathbf{X}_i = (x_{i1}, x_{i2}, \dots, x_{iq})^T$ denotes q covariates, such as age, gender and
 1084 ancestral principal components; $\mathbf{G}_i = (G_{i1}, G_{i2}, \dots, G_{ip})^T$ denotes the genotype matrix of
 1085 the p genetic variants in a variant set. Since these K phenotypes may be defined on
 1086 different measurement scales, we assume that each phenotype has been rescaled to
 1087 have zero mean and unit variance.

1088

1089 When the data consist of unrelated samples, we consider the following Multivariate
 1090 Linear Model (MLM)

$$\mathbf{Y}_i = \begin{bmatrix} y_{i1} \\ y_{i2} \\ \vdots \\ y_{iK} \end{bmatrix} = \begin{bmatrix} \alpha_{0,1} + \mathbf{X}_i^T \boldsymbol{\alpha}_1 + \mathbf{G}_i^T \boldsymbol{\beta}_1 \\ \alpha_{0,2} + \mathbf{X}_i^T \boldsymbol{\alpha}_2 + \mathbf{G}_i^T \boldsymbol{\beta}_2 \\ \vdots \\ \alpha_{0,K} + \mathbf{X}_i^T \boldsymbol{\alpha}_K + \mathbf{G}_i^T \boldsymbol{\beta}_K \end{bmatrix} + \begin{bmatrix} \varepsilon_{i1} \\ \varepsilon_{i2} \\ \vdots \\ \varepsilon_{iK} \end{bmatrix}, \#(1)$$

1091 where $\alpha_{0,k}$ is an intercept, $\boldsymbol{\alpha}_k = (\alpha_{1,k}, \alpha_{2,k}, \dots, \alpha_{q,k})^T$ and $\boldsymbol{\beta}_k = (\beta_{1,k}, \beta_{2,k}, \dots, \beta_{p,k})^T$ are
 1092 column vectors of regression coefficients for covariates \mathbf{X}_i and genotype \mathbf{G}_i in
 1093 phenotype k , respectively. The error terms $\boldsymbol{\varepsilon}_i = (\varepsilon_{i1}, \varepsilon_{i2}, \dots, \varepsilon_{iK})^T$ are independent and
 1094 identically distributed and follow a multivariate normal distribution with mean a vector of
 1095 zeros and variance-covariance matrix $\boldsymbol{\Sigma}_{K \times K}$, assumed identical for all subjects. For all n
 1096 subjects, using matrix notation we can write model (1) as

$$\mathbf{Y}_{n \times K} = \mathbf{1}_n \boldsymbol{\alpha}_0^T + \mathbf{X}_{n \times q} \boldsymbol{\alpha}_{q \times K} + \mathbf{G}_{n \times p} \boldsymbol{\beta}_{p \times K} + \boldsymbol{\varepsilon}_{n \times K}, \#(2)$$

1097 where $\mathbf{1}_n$ is a column vector of 1's with length n , $\boldsymbol{\alpha}_0 = (\alpha_{0,1}, \alpha_{0,2}, \dots, \alpha_{0,K})^T$ is a column
 1098 vector of regression intercepts, the k -th columns of $\boldsymbol{\alpha}_{q \times K}$ and $\boldsymbol{\beta}_{p \times K}$ are $\boldsymbol{\alpha}_k$ and $\boldsymbol{\beta}_k$,
 1099 respectively, and $\boldsymbol{\varepsilon}_{n \times K} = (\boldsymbol{\varepsilon}_1, \boldsymbol{\varepsilon}_2, \dots, \boldsymbol{\varepsilon}_n)^T \sim \text{MatrixNormal}_{n,K}(\mathbf{0}_{n \times K}, \mathbf{I}_{n \times n}, \boldsymbol{\Sigma}_{K \times K})$ follows a

1100 matrix normal distribution. We calculate the scaled residual for each subject on each
 1101 phenotype, defined as $\hat{\mathbf{e}}_{n \times K} = (\mathbf{Y}_{n \times K} - \hat{\boldsymbol{\mu}}_{n \times K})\hat{\boldsymbol{\Sigma}}_{K \times K}^{-1}$, where $\hat{\boldsymbol{\mu}}_{n \times K}$ (a matrix of fitted
 1102 values) and $\hat{\boldsymbol{\Sigma}}_{K \times K}$ are estimated under the null MLM $\mathbf{Y}_{n \times K} = \mathbf{1}_n \boldsymbol{\alpha}_0^T + \mathbf{X}_{n \times q} \boldsymbol{\alpha}_{q \times K} + \boldsymbol{\varepsilon}_{n \times K}$,
 1103 where no variant has any effect on any outcome.

1104

1105 When the data consist of related samples, we consider the following Multivariate Linear
 1106 Mixed Model (MLMM)^{19,47,48}

$$\mathbf{Y}_i = \begin{bmatrix} y_{i1} \\ y_{i2} \\ \vdots \\ y_{iK} \end{bmatrix} = \begin{bmatrix} \alpha_{0,1} + \mathbf{X}_i^T \boldsymbol{\alpha}_1 + \mathbf{G}_i^T \boldsymbol{\beta}_1 \\ \alpha_{0,2} + \mathbf{X}_i^T \boldsymbol{\alpha}_2 + \mathbf{G}_i^T \boldsymbol{\beta}_2 \\ \vdots \\ \alpha_{0,K} + \mathbf{X}_i^T \boldsymbol{\alpha}_K + \mathbf{G}_i^T \boldsymbol{\beta}_K \end{bmatrix} + \begin{bmatrix} b_{i1} \\ b_{i2} \\ \vdots \\ b_{iK} \end{bmatrix} + \begin{bmatrix} \varepsilon_{i1} \\ \varepsilon_{i2} \\ \vdots \\ \varepsilon_{iK} \end{bmatrix}, \quad \#(3)$$

1107 where the random effects b_{ik} account for relatedness and remaining population
 1108 structure unaccounted by ancestral PCs²⁰. We assume that $\mathbf{b}_{n \times K} = (b_{ik})_{n \times K} \sim$
 1109 MatrixNormal _{n, K} ($\mathbf{0}_{n \times K}$, $\boldsymbol{\Phi}_{n \times n}$, $\boldsymbol{\Theta}_{K \times K}$) with a variance component matrix $\boldsymbol{\Theta}_{K \times K}$ and a
 1110 sparse genetic relatedness matrix $\boldsymbol{\Phi}_{n \times n}$ ^{21,22}. For all n subjects, using matrix notation we
 1111 can rewrite equation (3) as

$$\mathbf{Y}_{n \times K} = \mathbf{1}_n \boldsymbol{\alpha}_0^T + \mathbf{X}_{n \times q} \boldsymbol{\alpha}_{q \times K} + \mathbf{G}_{n \times p} \boldsymbol{\beta}_{p \times K} + \mathbf{b}_{n \times K} + \boldsymbol{\varepsilon}_{n \times K}. \quad \#(4)$$

1112 We calculate the scaled residual for each subject on each phenotype, defined as
 1113 $\hat{\mathbf{e}}_{n \times K} = (\mathbf{Y}_{n \times K} - \hat{\boldsymbol{\mu}}_{n \times K})\hat{\boldsymbol{\Sigma}}_{K \times K}^{-1}$, where $\hat{\boldsymbol{\mu}}_{n \times K}$ and $\hat{\boldsymbol{\Sigma}}_{K \times K}$ are estimated under the null MLMM
 1114 $\mathbf{Y}_{n \times K} = \mathbf{1}_n \boldsymbol{\alpha}_0^T + \mathbf{X}_{n \times q} \boldsymbol{\alpha}_{q \times K} + \mathbf{b}_{n \times K} + \boldsymbol{\varepsilon}_{n \times K}$. Under both MLM and MLMM, our goal is to
 1115 test for an association between a set of p genetic variants and K quantitative
 1116 phenotypes, adjusting for covariates and relatedness. This corresponds to testing
 1117 $H_0: \boldsymbol{\beta}_1 = \boldsymbol{\beta}_2 = \cdots = \boldsymbol{\beta}_K = \mathbf{0}$.

1118

1119 **Multi-trait rare variant association tests using MultiSTAAR**

1120 Single-trait score-based aggregation methods⁵⁻⁹ can be extended to allow for jointly
1121 testing the association between rare variants in a variant set and multiple quantitative
1122 phenotypes. For a given variant set, let $\mathbf{S}_{p \times K} = (S_{jk})_{p \times K} = (\mathbf{G}_{n \times p})^T \hat{\mathbf{e}}_{n \times K}$ denote the
1123 matrix of score statistics where S_{jk} is the score statistic for the j -th variant on the k -th
1124 phenotype. For multi-trait burden test using MultiSTAAR (Burden-MT), we consider test
1125 statistic

$$Q_{Burden-MT} = \left(\sum_{j=1}^p w_j \mathbf{S}_{j \cdot} \right) \hat{\mathbf{V}}^{-1} \left(\sum_{j=1}^p w_j \mathbf{S}_{j \cdot} \right)^T,$$

1126 where w_j is the weight defined as a function of the MAF for the j -th variant^{4,18}, $\mathbf{S}_{j \cdot} =$
1127 $(S_{j1}, S_{j2}, \dots, S_{jK})$ is the j -th row of \mathbf{S} and $\hat{\mathbf{V}}$ is the estimated variance-covariance matrix of
1128 $\sum_{j=1}^p w_j \mathbf{S}_{j \cdot} = \mathbf{w}^T \mathbf{S}$. $Q_{Burden-MT}$ asymptotically follows a standard chi-square distribution
1129 with K degrees of freedom under the null hypothesis, and its P value can be obtained
1130 analytically while accounting for LD between variants and correlation between
1131 phenotypes.

1132

1133 For multi-trait SKAT using MultiSTAAR (SKAT-MT), we consider the statistic

$$Q_{SKAT-MT} = \sum_{k=1}^K \sum_{j=1}^p w_j^2 S_{jk}^2.$$

1134 $Q_{SKAT-MT}$ asymptotically follows a mixture of chi-square distributions under the null
1135 hypothesis, and its P value can be obtained analytically while accounting for LD
1136 between variants and correlation between phenotypes^{14,15}.

1137

1138 For multi-trait ACAT-V using MultiSTAAR (ACAT-V-MT), we propose test statistic

$$Q_{ACAT-V-MT} = \overline{w^2 \text{MAF}(1 - \text{MAF})} \tan((0.5 - p_0)\pi)$$

$$+ \sum_{j=1}^{p'} w_j^2 \text{MAF}_j (1 - \text{MAF}_j) \tan((0.5 - p_j)\pi),$$

1139 where p' is the number of variants with a minor allele count (MAC) greater than 10 and

1140 p_j is the multi-trait association P value of individual variant j for those variants with a

1141 MAC > 10, whose test statistic is given by the K degrees of freedom multivariate score

1142 test

$$Q_j = \mathbf{S}_{j\cdot} \widehat{\mathbf{V}}_{\mathbf{S}_{j\cdot}}^{-1} \mathbf{S}_{j\cdot}^T$$

1143 where $\widehat{\mathbf{V}}_{\mathbf{S}_{j\cdot}}$ is the estimated variance-covariance matrix of $\mathbf{S}_{j\cdot}$; p_0 is the multi-trait burden

1144 test P value of extremely rare variants with an MAC ≤ 10 as described above and

1145 $\overline{w^2 \text{MAF}(1 - \text{MAF})}$ is the average of the weights $w_j^2 \text{MAF}_j (1 - \text{MAF}_j)$ among the

1146 extremely rare variants with an MAC ≤ 10 . $Q_{ACAT-V-MT}$ is approximated well by a scaled

1147 Cauchy distribution under the null hypothesis, and its P value can be obtained

1148 analytically while accounting for LD between variants and correlation between

1149 phenotypes^{9,49}. Note that when $K = 1$, the multi-trait burden, SKAT, and ACAT-V tests

1150 reduce to the original single-trait burden, SKAT and ACAT-V tests.

1151

1152 Suppose we have a collection of L annotations, let A_{jl} denote the l -th annotation for the

1153 j th variant in the variant set. We define the functionally-informed multi-trait burden,

1154 SKAT and ACAT-V test statistics weighted by the l -th annotation as follows

$$Q_{Burden-MT,l,(a_1,a_2)} = \left(\sum_{j=1}^p \hat{\pi}_{jl} w_{j,(a_1,a_2)} \mathbf{S}_{j\cdot} \right) \widehat{\mathbf{V}}_{l,(a_1,a_2)}^{-1} \left(\sum_{j=1}^p \hat{\pi}_{jl} w_{j,(a_1,a_2)} \mathbf{S}_{j\cdot} \right)^T,$$

$$Q_{SKAT-MT,l,(a_1,a_2)} = \sum_{k=1}^K \sum_{j=1}^p \hat{\pi}_{jl} w_{j,(a_1,a_2)}^2 S_{jk}^2,$$

$$Q_{ACAT-V-MT,l,(a_1,a_2)}$$

$$= \overline{\hat{\pi}_{\cdot l} w_{(a_1,a_2)}^2 \text{MAF}(1 - \text{MAF})} \tan((0.5 - p_{0,l})\pi)$$

$$+ \sum_{j=1}^{M'} \hat{\pi}_{jl} w_{j,(a_1,a_2)}^2 \text{MAF}_j (1 - \text{MAF}_j) \tan((0.5 - p_j)\pi),$$

1155 where $\hat{\pi}_{jl} = \frac{\text{rank}(A_{jl})}{M}$, $w_{j,(a_1,a_2)} = \text{Beta}(\text{MAF}_j; a_1, a_2)$ with $(a_1, a_2) \in \mathcal{A} = \{(1,25), (1,1)\}$,

1156 $\widehat{\mathbf{V}}_{l,(a_1,a_2)}$ is the estimated variance-covariance matrix of $\sum_{j=1}^p \hat{\pi}_{jl} w_{j,(a_1,a_2)} \mathbf{S}_{j\cdot}$ and

1157 $\overline{\hat{\pi}_{\cdot l} w_{(a_1,a_2)}^2 \text{MAF}(1 - \text{MAF})}$ is the average of the weights $\hat{\pi}_{jl} w_{j,(a_1,a_2)}^2 \text{MAF}_j (1 -$

1158 $\text{MAF}_j)$ among the extremely rare variants with $\text{MAC} \leq 10$. Finally, we define the

1159 omnibus MultiSTAAR-O test statistic as

$$\begin{aligned} T_{MultiSTAAR-O} &= \frac{1}{3|\mathcal{A}|} \sum_{(a_1,a_2) \in \mathcal{A}} [T_{MultiSTAAR-B(a_1,a_2)} + T_{MultiSTAAR-S(a_1,a_2)} \\ &\quad + T_{MultiSTAAR-A(a_1,a_2)}] \\ &= \frac{1}{3|\mathcal{A}|} \sum_{(a_1,a_2) \in \mathcal{A}} \sum_{l=0}^L \left[\frac{\tan\{(0.5 - p_{Burden-MT,l,(a_1,a_2)})\pi\}}{L+1} \right. \\ &\quad \left. + \frac{\tan\{(0.5 - p_{SKAT-MT,l,(a_1,a_2)})\pi\}}{L+1} + \frac{\tan\{(0.5 - p_{ACAT-V-MT,l,(a_1,a_2)})\pi\}}{L+1} \right], \end{aligned}$$

1160 and the P value of $T_{MultiSTAAR-O}$ can be calculated by

$$p_{MultiSTAAR-O} = \frac{1}{2} - \frac{\{\arctan(T_{MultiSTAAR-O})\}}{\pi}.$$

1161

1162 **Data simulation**

1163 *Type I error rate simulations*

1164 We performed simulation studies to evaluate how accurately MultiSTAAR controls the
1165 type I error rate. We generated three quantitative traits from a multivariate linear model,
1166 conditional on two covariates

$$\mathbf{Y}_i = \begin{bmatrix} Y_{i1} \\ Y_{i2} \\ Y_{i3} \end{bmatrix} = \begin{bmatrix} 0.5X_{i1} + 0.5X_{i2} \\ 0.5X_{i1} + 0.5X_{i2} \\ 0.5X_{i1} + 0.5X_{i2} \end{bmatrix} + \begin{bmatrix} \varepsilon_{i1} \\ \varepsilon_{i2} \\ \varepsilon_{i3} \end{bmatrix},$$

1167 where $X_{i1} \sim N(0,1)$, $X_{i2} \sim \text{Bernoulli}(0.5)$ and

$$\begin{bmatrix} \varepsilon_{i1} \\ \varepsilon_{i2} \\ \varepsilon_{i3} \end{bmatrix} \sim MVN \left(\begin{bmatrix} 0 \\ 0 \\ 0 \end{bmatrix}, \begin{bmatrix} 1.0 & -0.1 & 0.2 \\ -0.1 & 1.0 & -0.4 \\ 0.2 & -0.4 & 1.0 \end{bmatrix} \right).$$

1168

1169 The correlation matrix of error terms $\varepsilon_i = (\varepsilon_{i1}, \varepsilon_{i2}, \varepsilon_{i3})^T$ was chosen to mimic the
1170 correlations between three lipid traits LDL-C, HDL-C and TG, estimated from the
1171 TOPMed data²⁶. We considered a sample size of 10,000 and generated genotypes by
1172 simulating 20,000 sequences for 100 different regions each spanning 1 Mb. The data
1173 generation used the calibration coalescent model (COSI)²⁹ with parameters set to mimic
1174 the LD structure of African Americans. In each simulation replicate, 10 annotations were
1175 generated as A_1, \dots, A_{10} all independently and identically distributed as $N(0,1)$ for each
1176 variant, and we randomly selected 5-kb regions from these 1-Mb regions for type I error
1177 rate simulations. We applied MultiSTAAR-B, MultiSTAAR-S, MultiSTAAR-A and
1178 MultiSTAAR-O by incorporating MAFs and the 10 annotations together with Burden-MT,

1179 SKAT-MT and ACAT-V-MT tests. We repeated the procedure with 10^8 replicates to
1180 examine the type I error rate at levels $\alpha = 10^{-4}, 10^{-5}$, and 10^{-6} .

1181

1182 *Empirical power simulations*

1183 Next, we carried out simulation studies under a variety of configurations to assess the
1184 the power of MultiSTAAR-O, and how its incorporation of multiple functional annotations
1185 affects power compared to the multi-trait burden, SKAT, and ACAT-V tests implemented
1186 in MultiSTAAR. In each simulation replicate, we randomly selected 5-kb regions from a
1187 1-Mb region for power evaluations. For each selected 5-kb region, we generated three
1188 quantitative traits from a multivariate linear model

$$\mathbf{Y}_i = \begin{bmatrix} Y_{i1} \\ Y_{i2} \\ Y_{i3} \end{bmatrix} = \begin{bmatrix} 0.5X_{i1} + 0.5X_{i2} + \mathbf{G}_i^T \boldsymbol{\beta}_1 \\ 0.5X_{i1} + 0.5X_{i2} + \mathbf{G}_i^T \boldsymbol{\beta}_2 \\ 0.5X_{i1} + 0.5X_{i2} + \mathbf{G}_i^T \boldsymbol{\beta}_3 \end{bmatrix} + \begin{bmatrix} \varepsilon_{i1} \\ \varepsilon_{i2} \\ \varepsilon_{i3} \end{bmatrix},$$

1189 where $X_{1i}, X_{2i}, \varepsilon_i$ were defined as in the type I error rate simulations,
1190 $\mathbf{G}_i = (G_{i1}, G_{i2}, \dots, G_{ip})^T$ and $\boldsymbol{\beta}_k = (\beta_{1,k}, \beta_{2,k}, \dots, \beta_{p,k})^T$ were the genotypes and effect sizes
1191 of the p genetic variants in the signal region.

1192

1193 The genetic effect of variant j on phenotype k was defined as $\beta_{j,k} = c_j d_k \gamma_j$ to allow for
1194 heterogeneous effect sizes among variants and phenotypes. Specifically, we generated
1195 the causal variant indicator c_j according to a logistic model

$$\text{logit } P(c_j = 1) = \delta_0 + \delta_{l_1} A_{j,l_1} + \delta_{l_2} A_{j,l_2} + \delta_{l_3} A_{j,l_3} + \delta_{l_4} A_{j,l_4} + \delta_{l_5} A_{j,l_5},$$

1196 where $\{l_1, \dots, l_5\} \subset \{1, \dots, 10\}$ were randomly sampled for each region. For different
1197 regions, causality of variants depended on different sets of annotations. We set
1198 $\delta_l = \log(5)$ for all annotations and varied the proportions of causal variants in the signal

1199 region by setting $\delta_0 = \text{logit}(0.0015)$, $\text{logit}(0.015)$ and $\text{logit}(0.18)$ which corresponds to
1200 averaging 5%, 15% and 35% causal variants in the signal region, respectively. We
1201 considered four scenarios of phenotypic indicator d_k that reflect different underlying
1202 genetic architectures across phenotypes: $(d_1, d_2, d_3) = (1, 0, 0)$, $(1, 0, 1)$, $(1, 1, 0)$ and
1203 $(1, 1, 1)$. These correspond to causal variants in the signal region being associated with
1204 (1) one phenotype only, (2) two positively correlated phenotypes, (3) two negatively
1205 correlated phenotypes and (4) all three phenotypes. We modeled the absolute effect
1206 sizes of causal variants using $|\gamma_j| = c_0 |\log_{10} MAF_j|$, such that it was a decreasing
1207 function of MAF. c_0 was set to be 0.13, 0.1, 0.1 and 0.07, respectively, to ensure a
1208 decent power of tests under each scenario. We additionally varied the proportions of
1209 causal variant effect size directions (signs of r_j) by randomly generating 100%, 80%,
1210 and 50% variants on average to have positive effects. We applied MultiSTAAR-B,
1211 MultiSTAAR-S, MultiSTAAR-A, and MultiSTAAR-O using MAFs and all 10 annotations
1212 together with Burden-MT, SKAT-MT and ACAT-V-MT tests. We repeated the procedure
1213 with 10^4 replicates to examine the power at level $\alpha = 10^{-7}$. The sample size was 10,000
1214 across all scenarios.

1215

1216 **Lipid Traits**

1217 Conventionally measured plasma lipids, including LDL-C, HDL-C, and triglycerides,
1218 were included for analysis. LDL-C was either calculated by the Friedewald equation
1219 when triglycerides were <400 mg/dl or directly measured. Given the average effect of
1220 statins, when statins were present, LDL-C was adjusted by dividing by 0.7. Triglycerides

1221 were natural log transformed for analysis. Phenotypes were harmonized by each cohort
1222 and deposited into the dbGaP TOPMed Exchange Area.

1223

1224 **Multi-trait analysis of lipid levels in the TOPMed WGS data**

1225 The TOPMed WGS data consist of multi-ethnic related samples¹. Race/ethnicity was
1226 defined using a combination of self-reported race/ethnicity from participant
1227 questionnaires and study recruitment information (**Supplementary Note**)³¹. In this
1228 study, we applied MultiSTAAR to perform multi-trait rare variant analysis of three
1229 quantitative lipid traits (LDL-C, HDL-C and TG) using 20 study cohorts from the
1230 TOPMed Freeze 8 WGS data. LDL-C was adjusted for the presence of medications as
1231 before³⁰. For each study, we first fit a linear regression model adjusting for age, age²,
1232 sex for each race/ethnicity-specific group. In addition, for Old Order Amish (OOA), we
1233 also adjusted for *APOB* p.R3527Q in LDL-C and TC analyses and adjusted for *APOC3*
1234 p.R19Ter in TG and HDL-C analyses³⁰.

1235

1236 We performed rank-based inverse normal transformation of the residuals of LDL-C,
1237 HDL-C and TG within each race/ethnicity-specific group. We then fit a multivariate linear
1238 mixed model for the rank normalized residuals, adjusting for 11 ancestral principal
1239 components, ethnicity group indicators, and a variance component for empirically
1240 derived sparse kinship matrix to account for population structure, relatedness and
1241 correlation between phenotypes.

1242

1243 We next applied MultiSTAAR-O to perform multi-trait variant set analyses for rare
1244 variants (MAF < 1%) by scanning the genome, including gene-centric analysis of each
1245 protein-coding gene using five coding variant functional categories (putative loss-of-
1246 function rare variants, missense rare variants, disruptive missense rare variants,
1247 putative loss-of-function and disruptive missense rare variants and synonymous rare
1248 variants); seven noncoding variant functional categories (promoter rare variants overlaid
1249 with CAGE sites, promoter rare variants overlaid with DHS sites, enhancer rare variants
1250 overlaid with CAGE sites, enhancer rare variants overlaid with DHS sites, UTR rare
1251 variants, upstream region rare variants, downstream region rare variants) and rare
1252 variants in ncRNA genes; and genetic region analysis using 2-kb sliding windows
1253 across the genome with a 1-kb skip length. The WGS multi-trait rare variant analysis
1254 was performed using the R packages MultiSTAAR (version 0.9.7,
1255 <https://github.com/xihaoli/MultiSTAAR>) and STAARpipeline (version 0.9.7,
1256 <https://github.com/xihaoli/STAARpipeline>). The WGS rare variant single-trait analysis of
1257 LDL-C, HDL-C and TG was performed using the R package STAARpipeline (version
1258 0.9.7, <https://github.com/xihaoli/STAARpipeline>). Both multi-trait and single-trait
1259 analyses results were summarized and visualized using the R package
1260 STAARpipelineSummary (version 0.9.7,
1261 <https://github.com/xihaoli/STAARpipelineSummary>).

1262

1263 **Genome build**

1264 All genome coordinates are given in NCBI GRCh38/UCSC hg38.

1265

1266 **Statistics and reproducibility**

1267 Sample size was not predetermined. The multi-trait analysis consists of 20 study
1268 cohorts of TOPMed Freeze 8 and had 61,838 samples with lipid traits. We did not use
1269 any study design that required randomization or blinding.

1270

1271 **Data availability**

1272 This paper used the TOPMed Freeze 8 WGS data and lipids phenotype data. Genotype
1273 and phenotype data are both available in database of Genotypes and Phenotypes. The
1274 TOPMed WGS data were from the following twenty study cohorts (accession numbers
1275 provided in parentheses): Old Order Amish (phs000956.v1.p1), Atherosclerosis Risk in
1276 Communities Study (phs001211), Mt Sinai BioMe Biobank (phs001644), Coronary
1277 Artery Risk Development in Young Adults (phs001612), Cleveland Family Study
1278 (phs000954), Cardiovascular Health Study (phs001368), Diabetes Heart Study
1279 (phs001412), Framingham Heart Study (phs000974), Genetic Study of Atherosclerosis
1280 Risk (phs001218), Genetic Epidemiology Network of Arteriopathy (phs001345), Genetic
1281 Epidemiology Network of Salt Sensitivity (phs001217), Genetics of Lipid Lowering
1282 Drugs and Diet Network (phs001359), Hispanic Community Health Study - Study of
1283 Latinos (phs001395), Hypertension Genetic Epidemiology Network and Genetic
1284 Epidemiology Network of Arteriopathy (phs001293), Jackson Heart Study (phs000964),
1285 Multi-Ethnic Study of Atherosclerosis (phs001416), San Antonio Family Heart Study
1286 (phs001215), Genome-wide Association Study of Adiposity in Samoans (phs000972),
1287 Taiwan Study of Hypertension using Rare Variants (phs001387), and Women's Health

1288 Initiative (phs001237). The sample sizes, ancestry and phenotype summary statistics of
1289 these cohorts are given in **Supplementary Table 2**.

1290

1291 The functional annotation data are publicly available and were downloaded from the
1292 following links: GRCh38 CADD v1.4 (<https://cadd.gs.washington.edu/download>);
1293 ANNOVAR dbNSFP v3.3a (<https://annovar.openbioinformatics.org/en/latest/user-guide/download>); LINSIGHT (<https://github.com/CshlSiepelLab/LINSIGHT>); FATHMM-
1294 XF (<http://fathmm.biocompute.org.uk/fathmm-xf>); FANTOM5 CAGE
1295 (<https://fantom.gsc.riken.jp/5/data>); GeneCards (<https://www.genecards.org>; v4.7 for
1296 [hg38](#)); and Umap/Bismap (<https://bismap.hoffmanlab.org>; ‘before March 2020’ version).
1297
1298 In addition, recombination rate and nucleotide diversity were obtained from Gazal et
1299 al⁵⁰. The whole-genome individual functional annotation data was assembled from a
1300 variety of sources and the computed annotation principal components are available at
1301 the Functional Annotation of Variant-Online Resource (FAVOR) site
1302 (<https://favor.genohub.org>)⁵¹ and the FAVOR database
1303 (<https://doi.org/10.7910/DVN/1VGTJI>)⁵².

1304

1305 **Code availability**

1306 MultiSTAAR is implemented as an open source R package available at
1307 <https://github.com/xihaoli/MultiSTAAR> and
1308 <https://content.sph.harvard.edu/xlin/software.html>. Data analysis was performed in R
1309 (4.1.0). STAAR v0.9.7 and MultiSTAAR v0.9.7 were used in simulation and real data
1310 analysis and implemented as open-source R packages available at

1311 <https://github.com/xihaoli/STAAR> and <https://github.com/xihaoli/MultiSTAAR>. The
1312 assembled functional annotation data were downloaded from FAVOR using Wget
1313 (<https://www.gnu.org/software/wget/wget.html>).
1314

1315 **References**

- 1316 50. Gazal, S. *et al.* Linkage disequilibrium–dependent architecture of human complex
1317 traits shows action of negative selection. *Nature Genetics* **49**, 1421-1427 (2017).
1318 51. Zhou, H. *et al.* FAVOR: functional annotation of variants online resource and
1319 annotator for variation across the human genome. *Nucleic Acids Research* **51**,
1320 D1300-D1311 (2023).
1321 52. Zhou, H., Arapoglou, T., Li, X., Li, Z. & Lin, X. FAVOR Essential Database. V1
1322 Edition (Harvard Dataverse, 2022).